

## Article

# Dynamics and Wear Prediction of Mechanisms Considering Multiple Clearances and Coatings

Qian Jing <sup>1,2,\*</sup> and Hongzhao Liu <sup>1</sup>

<sup>1</sup> School of Mechanical and Precision Instrument Engineering, Xi'an University of Technology, Xi'an 710048, China

<sup>2</sup> School of Mechanical Engineering, Long Dong University, Qingyang 745000, China

\* Correspondence: jingq@ldxy.edu.cn; Tel.: +86-(18)-209346537

**Abstract:** The increase in joint clearance and system vibration caused by joint wear are important factors that may lead to the failure of the mechanism and a decrease in the motion accuracy of the actuator. In this paper, to investigate the impact of different numbers of spherical joint clearances on the dynamics performance of the mechanism and explore effective measures to reduce the vibration of the mechanism caused by multiple joint clearances, on the basis of the previous research on the mechanism dynamics when there is clearance in a single spherical joint, an improved contact force model is used to study the effects of coating, no coating, and different clearance quantities on the dynamics of a mechanism containing multiple spherical joint clearances. Moreover, the joint reaction forces and contact-impact forces under different working conditions are calculated. In order to reduce the difficulty of calculating the joint wear, an approximate calculation method for contact area is proposed, and an improved Archard wear model is employed to calculate and analyze the changes in wear amount under the influence of both spherical joint clearance and coating.

**Keywords:** spherical joint clearance; coating; contact force model; dynamics; wear

## 1. Introduction

When all dynamic pairs in the mechanism are considered non-ideal joints, the dynamic calculation of the mechanism tends to become very difficult or even impossible [1]. Therefore, in the early stages of analyzing and studying the dynamics of clearance mechanisms, researchers often considered a single dynamic pair in a simple mechanism as a non-ideal joint and analyzed the impact of clearance on the mechanism dynamics by changing the parameter values in a single clearance joint. With the rapid development of computer technology and the continuous optimization of numerical calculation methods, to make the theoretical research on mechanisms with clearances more in line with practical working conditions, many scholars have begun to study mechanisms with multiple clearances and mixed clearances in recent years. For example, based on previous research on the mechanism dynamics containing a single rotating pair with clearances [2] and spherical joint clearance [3], Flores [4] proposed and discussed the modeling and analysis method for the dynamics of a multibody system containing multiple rotating pairs with clearances. With a typical planar crank slider mechanism as an example, Muvengei [5] investigated the influence of frictionless rotational clearance joints at different positions on the overall dynamic characteristics of a multibody system using the numerical method and analyzed the dynamic responses of various components of the system, including rotational clearance joints, under different clearance sizes and input speeds. On this basis, nine synchronous motion modes at the two rotational clearance joints and their impact on system dynamics performance were also thoroughly studied in this work [6]. With a planar four-bar mechanism containing three rotating pairs with clearances as an example, Mojtaba [7], Wang [8], and Geng [9] analyzed the dynamic characteristics of the planar mechanical



**Citation:** Jing, Q.; Liu, H. Dynamics and Wear Prediction of Mechanisms Considering Multiple Clearances and Coatings. *Lubricants* **2023**, *11*, 310.

<https://doi.org/10.3390/lubricants11070310>

Received: 22 June 2023

Revised: 17 July 2023

Accepted: 20 July 2023

Published: 22 July 2023



**Copyright:** © 2023 by the authors. Licensee MDPI, Basel, Switzerland. This article is an open access article distributed under the terms and conditions of the Creative Commons Attribution (CC BY) license (<https://creativecommons.org/licenses/by/4.0/>).

system containing rotating joints with clearances. Tan [10] investigated the dynamic characteristics of a crank slider mechanism containing single and double rotating joints with clearance. The study showed that there is a significant intercoupling region between two clearance joints, and the dynamic response of a mechanism with two clearance joints is not a simple combination of the dynamic responses of two mechanisms with one clearance joint. Therefore, all joints in a multibody system should be modeled as clearance joints. In order to explore the effects of mixed clearances on the dynamic characteristics of the multibody system, Wang [11] established a dynamics model of the multibody system that includes both rotating pair clearances and sliding pair clearances and analyzed the influence of mixed clearances on the dynamic characteristics of the crank slider mechanism. Yu [12] conducted a comprehensive study on the dynamic model and performance of an overconstrained planar parallelogram mechanism with multiple clearances, and the results showed that the clearance joints associated with redundant constraints have a significant impact on computational efficiency. The redundant constraints can reduce the contact impact of the system, thereby weakening its vibration. In [13], on the basis of variational inequalities, Hamilton's variational principle is employed to solve the dynamic characteristics of a crank slider mechanism containing three rotating pairs with clearances, and their results are compared with the Automatic Dynamic Analysis of Mechanical Systems (ADAMS) calculation results to verify the correctness of the method proposed in this work. The above works have conducted in-depth research on the dynamic performance of the mechanism containing multiple clearances with joints and obtained the numerical calculation methods for different numbers and types of dynamic pairs. However, it is not difficult to find that most of the above research focuses on the clearance between rotating pairs; some of them investigate the clearances between sliding pairs, and most of these methods are numerical calculation methods based on a planar mechanism. At present, there are not many works exploring the dynamics of the multi-clearance mechanism considering spherical joints, and further research should be carried out to investigate the dynamics of the mechanism containing spherical joint clearances.

Due to its low evaporation rate, wide range of operating temperatures, radiation resistance, corrosion resistance, and other advantages, solid lubrication is effective for the mechanism surface and joint clearance. Kou [14] prepared the  $ZrO_2$  coating on the surface of a steel ball using plasma spraying and analyzed the original surface and worn surface of samples using the 3D surface profiler and scanning electron microscope, and the results proved that the coating could provide good wear reduction and wear resistance properties to the surface of spherical hinges. By adopting the constitutive laws proposed by Ambrósio and Veríssimo [15], Silva [16] tried to reduce the vibration and wear of the mechanism by adding bushings. In this work, the dynamic results of the spherical hinge in various states were analyzed and compared, including the ideal state, non-lubricated clearance, lubricated clearance, and with bushings, and the performance of their method was verified by using the space four-bar mechanism and automotive suspension as examples. By considering the femur and acetabulum of the human hip joint as the ball and shell, Mohammed A. [17] added the Polyvinyl Alcohol (PVA) coatings to the clearances between the artificial femur and acetabulum caused by long-term wear layer by layer so as to reduce the wear at the joint clearances. The experimental results proved that wear-resistant coatings can reduce wear and vibration in the clearances, but this experiment has high requirements for the preparation process of coatings. Li [18] employed the absolute node coordinate method to establish a contact force model of the rotating pair considering both the flexibility of the bar and the solid coating, analyzed in detail the effects of different solid coating materials and recovery coefficients on the dynamics of the solar array system, and predicted the wear of the rigid body system and the rigid-flexible coupling system. At present, there is little dynamic research that considers both the mechanism clearance and the coating, and there are few reports on wear prediction on this basis. To fill this clearance, this study mainly investigates the dynamics of the mechanism containing spherical joint clearances under the

coating lubrication without discussing the specific properties and preparation methods of the coating material. The same coating materials used in [19] are also selected in this work.

Although the wear amount at the joint clearance of the mechanism can be measured through experiments, the experimental methods used to obtain the wear amount are often too expensive, or the experimental results cannot meet the actual requirements in engineering. Therefore, numerical calculation methods considering the friction model have been widely adopted in recent years. With a planar mechanism as an example, Zhuang [20] proposed an efficient wear prediction method based on multibody dynamics, considering irregular wear in rotating pairs under different driving conditions, mechanism dimensions, and clearance sizes, and they also made a parameterized description of the clearance boundary. Wang [21] predicted the impact of spherical joint clearance caused by wear on the dynamic performance of space mechanisms by establishing an Archard wear model and the multibody system motion equation. Zhuang [22] proposed a hybrid model based on the Archard wear model for predicting individual rotational joints under the three lubrication conditions of full film lubrication, boundary lubrication, and no lubrication, and this work provides a research idea for calculating the wear amount under fluid lubrication. In [18,23], with the solar cell array and the 3RSR parallel mechanism as examples, the Archard wear model was used to calculate the wear amount at specific rotating pair and spherical joint clearances. At present, most of the numerical calculation methods for wear amounts are based on the Archard wear model. In order to reduce the difficulty of joint wear calculation, an approximate calculation method of contact area is proposed in this paper. A differential form of the Archard wear model is used to study the dynamic wear characteristics of the mechanism containing spherical joint clearances and coating.

Based on previous research on the dynamics of mechanisms containing single clearances, this work mainly investigates the dynamics and joint wear of space mechanisms considering both coatings and multiple spherical joint clearances, analyzes the impact of joint clearances on the dynamic performance of the mechanism in actual working conditions, and verifies the effectiveness of coatings in reducing system vibration caused by joint clearances and the wear reduction effect of coating lubrication characteristics on the mechanism. The specific structure of this paper is as follows:

- (i). The research background and significance of this work are introduced, mainly including the current research on the dynamics of multi-clearance joint mechanisms, the effects of solid lubrication coatings on vibration reduction and wear resistance of mechanisms, as well as the common methods and improvement measures for wear calculation;
- (ii). The method for determining the contact state, including the spherical joint clearances, is briefly described. The variable stiffness coefficient and viscous damping coefficient of the coating are utilized to obtain the contact-impact force at various joint clearances, and a dynamic model of the mechanism with multiple spherical joint clearances is established;
- (iii). On the basis of solving the dynamics of the mechanism containing multiple clearances, in order to reduce the difficulty of calculating joint wear, an approximate calculation method for the contact area is proposed. The improved Archard wear model is used to calculate the joint wear of a mechanism containing multiple joint clearances;
- (iv). With a space four-bar mechanism as the research object, the acceleration of the actuator (slider) and the wear change of the clearance joint when there are multiple spherical joint clearances in the mechanism are analyzed in detail. On this basis, the dynamics and wear change of the mechanism before and after the addition of coating to the joint clearances are compared, and the results demonstrate the feasibility of using coatings to reduce vibration and wear of the mechanism;
- (v). The main research contents and innovations of this paper are summarized, and the solution for the dynamics of mechanisms considering spherical joint clearances and the effectiveness of coatings in reducing the wear of spherical joint clearances are

concluded. This study can provide a feasible strategy to reduce vibration and increase the service life of the space deployable mechanism, considering joint clearances.

## 2. Dynamics of Mechanisms Containing Multiple Spherical Joint Clearances

### 2.1. Description: Spherical Joint Clearances

In this study on the dynamics of mechanisms containing clearances, the dynamic characteristics of various components in the mechanism considering joint clearances are analyzed, which can provide a theoretical basis for optimizing the structural parameters of the mechanism according to practical working conditions and ensure the stable performance, operation without fault, and long service life of the mechanism under set accuracy. On the basis of solving the dynamics of the ideal mechanism, the key to the dynamics of the mechanism considering spherical joint clearances is how to accurately describe the contact collision process when the spherical joint is between the ball and the spherical shell. The common structure of spherical joint clearance is shown in Figure 1. When considering the clearance, the geometric centers of shell  $i$  and ball  $j$  in motion generally do not coincide.  $O$ - $XYZ$ ,  $O_i$ - $\zeta_i\eta_i\zeta_i$ , and  $O_j$ - $\zeta_j\eta_j\zeta_j$  represent the coordinate systems of the mechanism, and the local coordinate systems of shell  $i$  and ball  $j$ , respectively;  $R_i$  and  $R_j$  represent the radiuses of shell  $i$  and ball  $j$ ;  $S_i^p$  and  $S_j^p$  are the length vectors from the geometric centers of shell  $i$  and ball  $j$  to the centroid of the component in the local coordinate system;  $r_i^p$  and  $r_j^p$  represent the vector diameters of the geometric centers of shell  $i$  and ball  $j$  in the global coordinate system; and  $r_i$  and  $r_j$  are the vector diameters of the centroids of the two components of the spherical joint in the global coordinate system. According to the geometric relationship in the figure, it is evident that:

$$\mathbf{r}_k^p = \mathbf{r}_k + \mathbf{A}_k \mathbf{S}_k^p \quad (k = i, j) \tag{1}$$

where  $\mathbf{A}_k$  is the transformation matrix of the local coordinates  $O_k$ - $\zeta_k\eta_k\zeta_k$  to the global coordinates  $O$ - $XYZ$ . Then, the eccentricity vector is:

$$\mathbf{e} = \mathbf{r}_i^p - \mathbf{r}_j^p \tag{2}$$

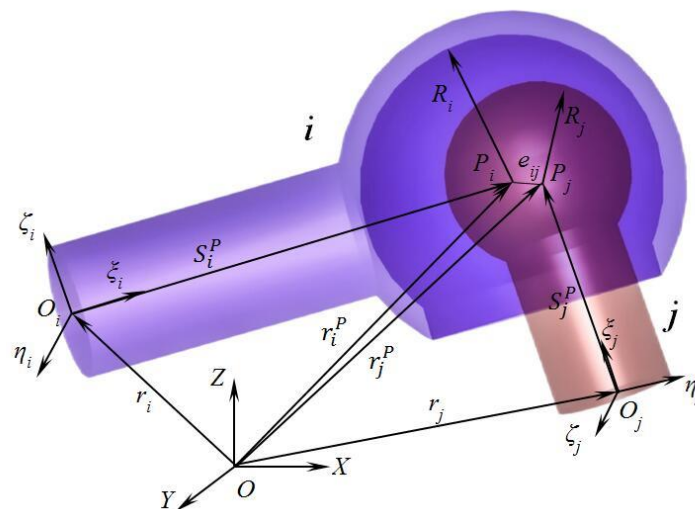


Figure 1. Spherical joint with clearance.

The collision direction vector between shell  $i$  and ball  $j$  can be obtained according to eccentricity:

$$\mathbf{n} = \frac{\mathbf{e}}{|\mathbf{e}|} \tag{3}$$

If the spherical joint clearance  $c$  is known, the depth of contact collision can be obtained as follows:

$$\delta = e - c. \tag{4}$$

Equation (4) can be used as the standard for contact detection, and its criteria are as follows:

$$\begin{cases} \delta < 0 & \text{Uncontacted, Free motion} \\ \delta = 0 & \text{Critical contact} \\ \delta > 0 & \text{Contact and deformation} \end{cases}.$$

This study is carried out based on previous research on the dynamics of the mechanism containing a single spherical joint clearance, and the Augmented Lagrangian Method is used for dynamic calculation. The dynamic calculation of the multi-clearance mechanism includes the following four steps [24]: (1) based on the position vector of the geometric center of contact element, the actual eccentricity distance  $e$  between the ball and shell of each spherical joint clearance is calculated, and the normal direction  $n$  and tangential direction  $t$  of the contact position between the ball and shell are determined; (2) the contact deformation  $\delta$  is calculated according to the given clearance value  $c$ , which is used to determine the contact state of the contact body; (3) the relative normal velocity  $v_n$  and tangential velocity  $v_t$  between the clearance joints are obtained according to the contact deformation  $\delta$ , and then  $v_n$  and  $v_t$  are substituted into the contact force model to obtain the contact forces of all spherical joint clearances at different moments of contact; and (4) the geometric constraints at all contact joints are replaced with the contact forces, and a dynamic model of the multi-clearance joint mechanism is established. The dynamic model of the multi-clearance joint mechanism can be represented as [25]:

$$\begin{bmatrix} \mathbf{M} & \mathbf{C}_q^T \\ \mathbf{C}_q & \mathbf{0} \end{bmatrix} \begin{bmatrix} \ddot{\mathbf{q}} \\ \lambda \end{bmatrix} = \begin{bmatrix} \mathbf{Q}_e + \sum_{i=1}^n \mathbf{F} \\ \gamma - 2\alpha\dot{\mathbf{C}} - \beta^2\mathbf{C} \end{bmatrix}, \tag{5}$$

where  $\mathbf{M}$  is the mass matrix of rigid body;  $\mathbf{C}_q$  is the Jacobian matrix of the mechanism;  $\ddot{\mathbf{q}}$  is the acceleration vector of generalized coordinates;  $\lambda$  is the Lagrange multiplier vector corresponding to the number of constraint equations;  $\mathbf{Q}_e$  is the generalized external force vector; and  $\sum_{i=1}^n \mathbf{F}$  is the sum of force vectors after the collision force vectors at  $n$  clearance hinges of the mechanism are converted to the centroid of the contact component when the side effects of clearance movement are considered in the mechanism;  $i$  represents the  $i$ -th clearance; and  $\gamma$  represents the quadratic term of velocity corresponding to the generalized coordinates. In order to overcome the constraint violation in the equation, the Baumgarte stabilization method [26] is employed, and good violation correction effects can be achieved when the correction coefficients  $\alpha$  and  $\beta$  are between 5 and 50. As for the algorithms of variable stiffness coefficient and viscous damping coefficient affected by the coating material and thickness in the contact force model, please refer to [19], which will not be elaborated here. The expressions of the variable stiffness coefficient, the viscous damping coefficient, and an improved contact force model are shown in Table 1.

**Table 1.** Contact force in joint clearance.

Contact Force	Variable Stiffness Coefficient	Viscous Damping Coefficient	Expression
$F_c$	$k_N = \frac{4\pi E_w^* R_2}{5} \frac{2\delta\Delta R + \delta^2}{(\Delta R + \delta)^2}$	$\chi_N = \frac{20k_N(1-c_r)}{13\alpha c_r \delta}$	$F_c = k_N\delta^n + \chi_N\delta^n\dot{\delta}$

In order to study the influence of coating material on the dynamic performance of mechanisms containing spherical joints with clearance, the equivalent modulus of double elastic layers was established by using the method of establishing a contact force model

with double elastic layers based on the Winkler elastic foundation model and the hypothesis of elliptic pressure distribution in Hertz theory. The improved variable stiffness coefficient of contact force is expressed as:

$$k_N = \frac{4\pi E_w^* R_2}{5} \frac{2\delta\Delta R + \delta^2}{(\Delta R + \delta)^2},$$

$$\frac{1}{E_w^*} = \frac{1 - \nu_i^2}{E_i^*} + \frac{1 - \nu_j^2}{E_j^*},$$

$$E_i^* = E_c^* E_s^* / (E_s^* l_c + E_c^* l_s),$$

$$E_{c,s}^* = \frac{E_{c,s}(1 - \nu_{c,s})}{(1 + \nu_{c,s})(1 - 2\nu_{c,s})},$$

where  $R_2$  represents the inner radius of the spherical shell,  $E^* w$  represents the equivalent elastic modulus of the double elastic layer,  $E^* c$  and  $E^* s$ , respectively, represent the equivalent elastic modulus of the coating and elastic modulus of the base,  $\nu^* c$  and  $\nu^* s$ , respectively, represent Poisson's ratio of the coating and base, and  $l_c$  and  $l_s$ , respectively, represent the thickness of the coating and base in millimeters. The 3D physical model of the spherical joint with clearance and coating is shown in Figure 2a, and the contact model with a double elastic layer is shown in Figure 2b.

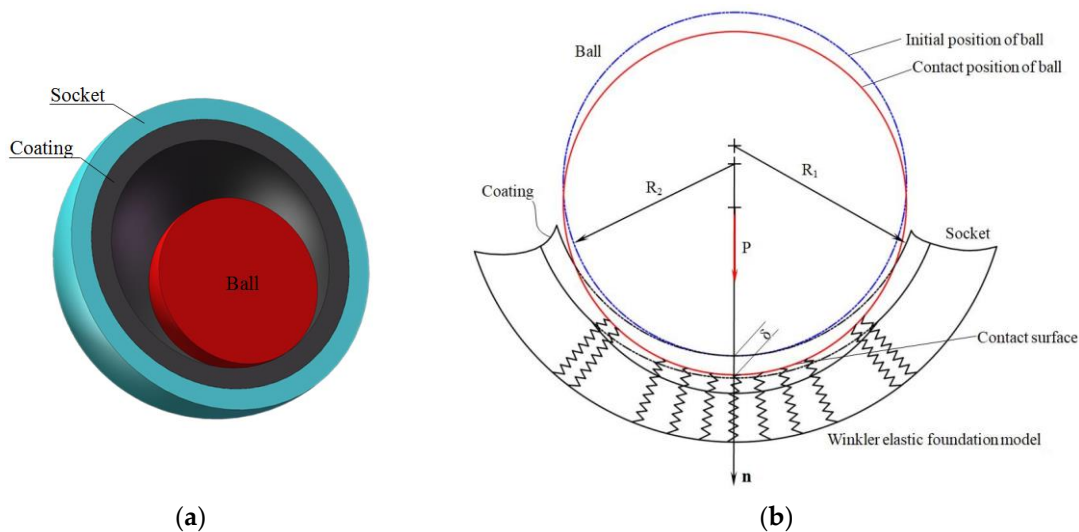


Figure 2. Double elastic layer contact model: (a) Physical model. (b) Geometrical model.

### 2.2. Transformation of Contact force between Spherical Joints

After obtaining the contact force  $F_c$  of the spherical joint, it needs to be converted into the system coordinate system before being substituted into the dynamic Equation (5) for calculation. When the contact forces  $F_{ic} = [f_{ix}, f_{iy}, f_{iz}]^T$  and  $F_{jc} = [f_{jx}, f_{jy}, f_{jz}]^T$  of contact elements  $i$  and  $j$  at the contact points  $Q_i$  and  $Q_j$  are moved to the centroids of the corresponding components, the eccentricities are as shown in Figure 3. After the contact force of the centroids of the two contact elements on the impact point of the shell is converted to the centroid, the force/moment can be expressed as:

$$\begin{cases} F_i = F_c \\ M_i = F_i \times (r_{Q_i} - r_i) \end{cases} \quad (6)$$

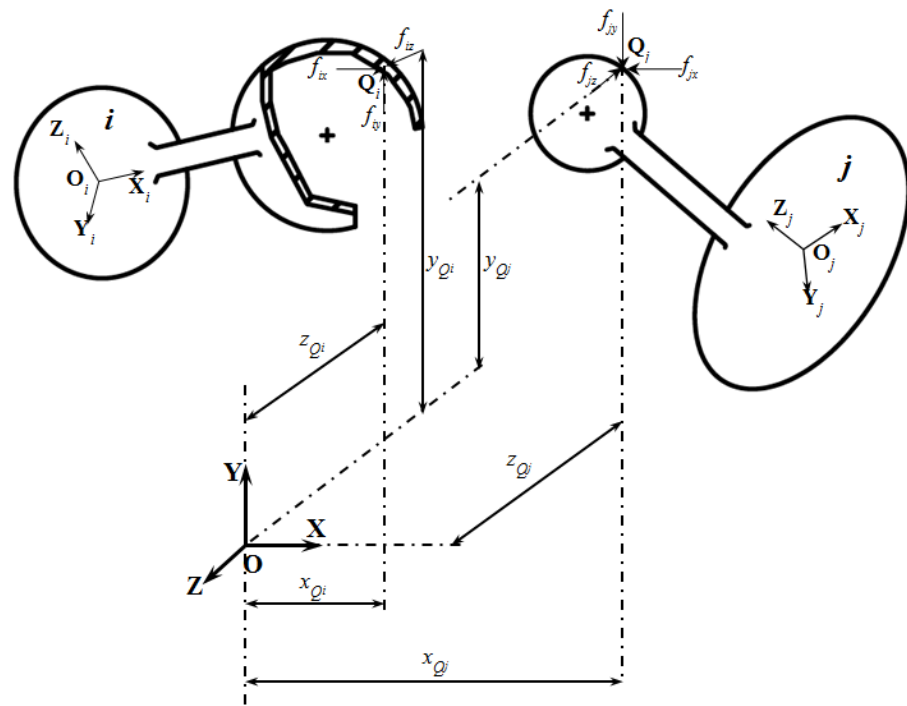


Figure 3. The transformation of contact force in a sphere joint.

The contact force acting on the ball and the contact force acting on the shell are mutually action and reaction. Therefore, the force and moment at the contact point of the ball after being converted to the centroid can be expressed as:

$$\begin{cases} \mathbf{F}_j = -\mathbf{F}_c \\ \mathbf{M}_j = \mathbf{F}_j \times (\mathbf{r}_{Q_j} - \mathbf{r}_j) \end{cases} \quad (7)$$

In Equations (6) and (7),  $\mathbf{r}_i$  and  $\mathbf{r}_j$  represent the position vectors of the contact element centroids in the global coordinate system, respectively;  $\mathbf{r}_{Q_i}$  and  $\mathbf{r}_{Q_j}$  represent the position vectors of the contact impact points in the global coordinate system. Their scalar form can be represented by Equation (8), and its form is shown in Figure 3.

$$\begin{cases} \mathbf{r}_{Q_i} = [x_{Q_i} \ y_{Q_i} \ z_{Q_i}]^T \\ \mathbf{r}_{Q_j} = [x_{Q_j} \ y_{Q_j} \ z_{Q_j}]^T \end{cases} \quad (8)$$

### 3. Wear of a Multi-Clearance Spherical Joint

Wear is the process of continuous damage to the surface materials caused by contacting objects in relative motion, which is an inevitable result of friction. Wear is not only related to the geometric characteristics of the contact body and the physical and chemical properties of the material but also to the contact temperature of the contact body and the dynamic load on the contact surface. However, since the experimental methods for obtaining the wear amount often involve high costs, the numerical calculation method considering the friction loss model has been adopted by scholars in recent years. For instance, Wang [21] predicted the impact of the spherical joint clearances caused by wear on the dynamic performance of the space multibody system based on the Archard wear model and the motion equation of the multibody system. By considering the three lubrication conditions of full film lubrication, boundary lubrication, and dry contact, Zhuang [22] proposed a hybrid model based on the Archard wear model, which was used to predict the wear of a single rotating joint under different lubrication conditions, thus providing an approach for predicting wear

under fluid lubrication. In [18,23], the analysis method based on the Archard wear model is also used, and with the solar cell arrays and 3RSR parallel mechanism as examples, the wear amounts at the clearances between the rotating pair and the spherical joint are calculated. At present, when the numerical calculation method is considered for the calculation of the wear amount, the Archard wear model is usually employed. In order to explore the change in wear amount with the contact-impact force, the differential form of the Archard wear model is used to study the dynamic wear characteristics of the hybrid clearance mechanism in this section.

### 3.1. Wear Model

The components of the mechanism experience friction and wear due to relative motion. When considering the joint clearance, the wear of contact elements is intensified under the contact-impact force. The commonly used Archard wear model is based on experimental measurements, which are related to the wear coefficient, slip distance, contact force, and material properties. Its specific expression is as follows [27]:

$$V = K_W \frac{F_N S}{H}, \tag{9}$$

where  $V$  is the wear volume,  $K_W$  is the wear coefficient,  $F_N$  is the contact-impact force,  $S$  is the relative slip distance of the contact surface, and  $H$  is the hardness of the contact material. Generally, for the purpose of simplifying calculation, the wear depth is used to replace the wear volume, so the above equation can be written as follows:

$$h_W = K_W \frac{F_N S}{HA} = \frac{k F_N S}{A}, \tag{10}$$

where  $h_W$  represents the depth of wear,  $A$  represents the contact area, and  $k$  is defined as the linear wear coefficient, which can be found in [28]. It should be noted that this study assumes that the surface roughness of the contact element is low and that the impact of material wear on the surface roughness is not considered; therefore, abrasive wear is not considered. According to the above equation, after obtaining the contact-impact force, the key to calculating the wear depth is to calculate the slip distance and contact area. The instantaneous state of collision between spherical joint elements is shown in Figure 4.

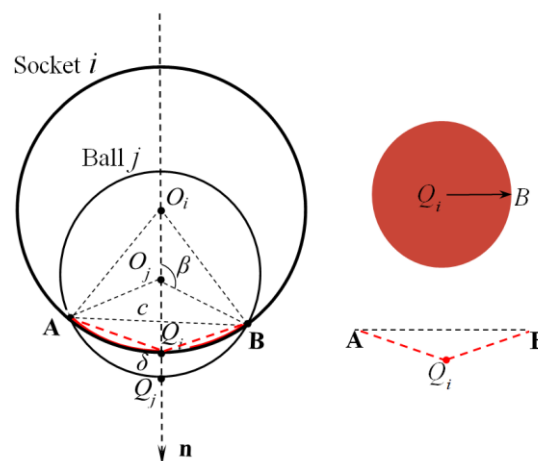


Figure 4. Contact collision model of a sphere joint.

Where  $O_i$  and  $O_j$  represent the geometric centers of the shell and ball, respectively;  $Q_i$  and  $Q_j$  represent the contact-impact points of the shell and ball;  $\delta = |Q_i - Q_j|$  represents the collision depth; and points A and B are the contact boundary points. If the radii of the

shell and ball are represented by  $R_i$  and  $R_j$ , according to the geometric relationship in the figure, we can obtain:

$$\beta = \arccos \left[ \frac{(\delta + R_i - R_j)^2 + R_j^2 - R_i^2}{2R_j(\delta + R_i - R_j)} \right], \quad (11)$$

and the contact depth can be obtained by:

$$h = |cQ_i| = R_j[1 - \cos(\pi - \beta)]. \quad (12)$$

At this point, the actual contact area is the spherical crown, with AB as the contact boundary. Because the actual collision depth is small, the surface area of the spherical crown is approximated using the cone  $Q_iAB$ , as shown in Figure 4, and the contact area is the circular area with  $Q_i$  as the center and  $|Q_iB|$  as the radius. The specific calculation is as follows:

$$A = \pi|Q_iB|^2 = \pi(|cB|^2 + h^2) \quad (13)$$

where  $|cB| = R_j \sin(\pi - \beta)$ . The slip distance  $S$  can be represented by the arc length corresponding to the increment of the relative rotation angle between the two contact bodies, and the increment of the relative rotation angle can be approximated by the increment  $\beta$  in Figure 4. Therefore, the expression of slip distance can be obtained as follows:

$$\Delta S = R_i \Delta \beta. \quad (14)$$

Substituting Equations (13) and (14) into Equation (10), the increment of contact wear depth can be obtained:

$$\Delta h_W = \frac{kF_N \Delta S}{A}. \quad (15)$$

According to the calculation of the increment of wear depth in the above equation, the numerical solution of the wear amount during the simulation period can be obtained through continuous superposition of the step sizes during the dynamic solution process and gradual accumulation of the wear depth.

The normal contact force can be separated into three contact force components along the system coordinates, according to Figure 5:

$$\begin{cases} F_{Nx} = F_N \sin \theta_z \cos \theta_x \\ F_{Ny} = F_N \sin \theta_z \sin \theta_x \\ F_{Nz} = F_N \cos \theta_z \end{cases}, \quad (16)$$

where  $F_N$  represents the normal contact force, and the azimuth angles  $\theta_x$ ,  $\theta_y$ , and  $\theta_z$  in the normal direction of the system coordinates can be calculated according to the eccentricity components  $e_x$ ,  $e_y$ , and  $e_z$  of the vector  $e$  in Equation (3), respectively:

$$\begin{cases} \theta_x = \arctan \frac{e_y}{e_x} \\ \theta_z = \arccos \frac{e_z}{e} \end{cases}. \quad (17)$$

### 3.2. Prediction of Multi-Clearance Wear

In this paper, the wear resistance of the solid lubrication coating is discussed, mainly considering that the selected material of the coating has a good self-lubricating performance, which reduces friction on the surface of the contact element with the coating in the case of contact collision. Without loss of generality, wear during contact collisions will be significantly reduced due to the lower wear coefficient. In order to study the effects of coating and clearance on joint wear of the mechanism, polytetrafluoroethylene (PTFE) with excellent lubrication, wear resistance, and relative adhesion performance is selected

as the coating material. Based on the preliminary analysis and study of the dynamics of the mechanism containing spherical joint clearances, the wear amounts of the mechanism considering spherical joint clearances at different positions and quantities, with coatings and without coatings, are calculated.

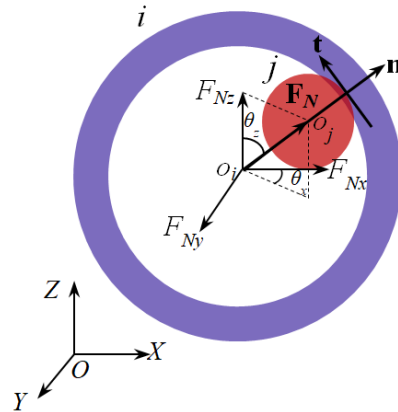


Figure 5. Contact force vector of spherical clearance joints.

In [19], a nonlinear stiffness coefficient expression and an improved viscous damping coefficient expression considering the wear reduction properties of coatings were proposed to obtain a conformal contact force model based on the analysis and comparison of the existing common normal contact force models shown in Table 1. The derivation and verification of the contact force model is the first part of the research considering spherical joint clearance and coating. Therefore, this contact force model is still selected for the dynamic calculation of multiple spherical joint clearances in this paper. At the initial stage of the dynamic analysis, the geometric parameters are modified through the calculation of the wear depth. The modified geometric model is substituted into the dynamic calculation process to determine the contact state in the next step. This process repeats until the end of the simulation. The specific analysis and calculation process is shown in the flow chart in Figure 6.

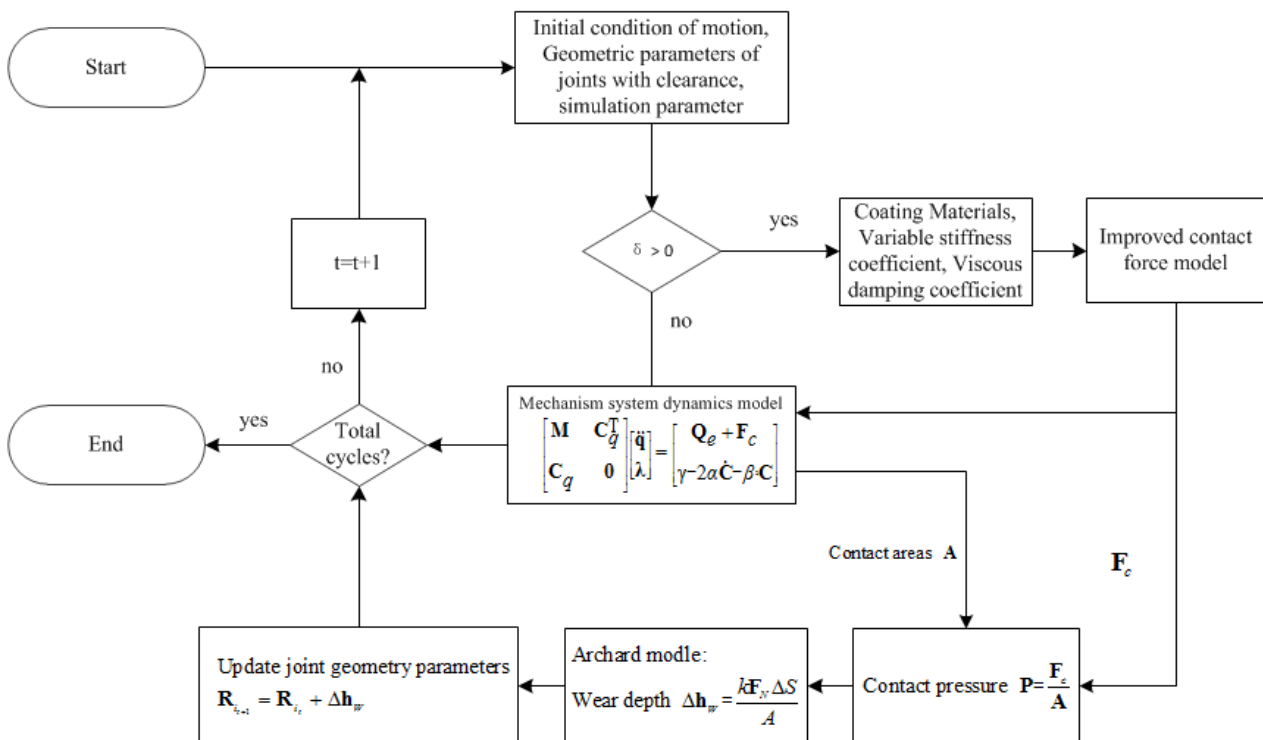


Figure 6. Wear prediction of spherical clearance joints.

### 4. Numerical Examples

#### 4.1. Mechanism Dynamics

In order to verify the effectiveness and correctness of the contact force model proposed in this section in solving the dynamic process of a space deployable mechanism considering spherical joint clearance and coating, a space four-bar mechanism RSSP is used as an example. The local coordinate system corresponding to each member bar  $l_i$  of the mechanism is  $O_i - X_i Y_i Z_i$  ( $i = 2, 3, 4$ ), and the global coordinate system is  $O - XYZ$ . The specific form and 3D structure of each coordinate system are shown in Figure 7. The generalized coordinates of the mechanism are defined as follows:

$$\mathbf{q} = [\mathbf{q}_2^T, \mathbf{q}_3^T, \mathbf{q}_4^T]^T, \mathbf{q}_i = [\mathbf{r}_i^T, \boldsymbol{\varphi}_i^T]^T \quad (i = 2, 3, 4), \tag{18}$$

where  $\mathbf{r}_i = [x_i, y_i, z_i]^T$  represents the position vector of the local coordinates  $O_i - X_i Y_i Z_i$  relative to the global coordinate system  $O - XYZ$ .

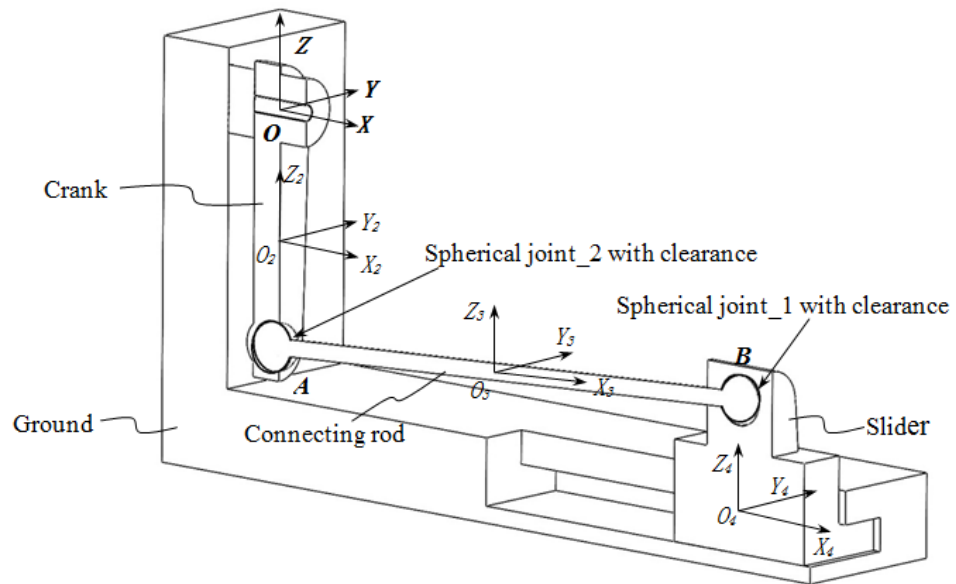


Figure 7. Space four-bar mechanism.

$\boldsymbol{\varphi}_i = [\alpha_i, \beta_i, \gamma_i]^T$  is the rotation vector of the local coordinate system relative to a fixed coordinate system. The Z-Y-X type Euler angles are used to describe the motion of the local coordinate system relative to the fixed coordinate system. The transformation matrix of each component is  $\mathbf{R}$ , and the expression is as follows:

$$\mathbf{R}_i = \mathbf{R}_i(\alpha_i, \beta_i, \gamma_i) = \mathbf{R}_z(\alpha_i)\mathbf{R}_y(\beta_i)\mathbf{R}_x(\gamma_i). \tag{19}$$

When there is a clearance between the spherical joint-1 and spherical joint-2 of the space four-bar mechanism, as shown in Figure 7, the constraint equation of the mechanism includes the following parts:

- (1) Constraint equation for an O-point ideal rotating pair:

$$\mathbf{C}_o = \mathbf{r}_2 + \mathbf{R}_2 \mathbf{s}_{o_2} - \mathbf{r}_1 - \mathbf{R}_1 \mathbf{s}_{o_1} = \mathbf{0}_{3 \times 1}, \tag{20}$$

the vectors in the above equation can be written as follows:

$$\mathbf{r}_2 = [x_2 \quad y_2 \quad z_2]^T, \mathbf{s}_{o_2} = [0 \quad 0 \quad \frac{l_2}{2}]^T, \mathbf{r}_1 = [0 \quad 0 \quad 0]^T, \mathbf{s}_{o_1} = [0 \quad 0 \quad 0]^T, \mathbf{R}_1 = \begin{bmatrix} 1 & 0 & 0 \\ 0 & 1 & 0 \\ 0 & 0 & 1 \end{bmatrix};$$

- (2) Constraint equation for an A-point ideal spherical joint:

$$\mathbf{C}_A = \mathbf{r}_3 + \mathbf{R}_3 \mathbf{s}_{A_3} - \mathbf{r}_2 - \mathbf{R}_2 \mathbf{s}_{A_2} = \mathbf{0}_{3 \times 1}, \tag{21}$$

the vectors in the above equation can be written as follows:

$$\mathbf{r}_3 = [x_3 \ y_3 \ z_3]^T, \mathbf{s}_{A_3} = [-\frac{l_3}{2} \ 0 \ 0]^T, \mathbf{s}_{A_2} = [0 \ 0 \ -\frac{l_2}{2}]^T;$$

(3) Constraint equation for a B-point ideal spherical joint:

$$\mathbf{C}_B = \mathbf{r}_4 + \mathbf{R}_4 \mathbf{s}_{B_4} - \mathbf{r}_3 - \mathbf{R}_3 \mathbf{s}_{B_3} = \mathbf{0}_{3 \times 1}, \tag{22}$$

the vectors in the above equation can be written as follows:

$$\mathbf{r}_4 = [x_4 \ 0 \ z_4]^T, \mathbf{s}_{B_4} = [0 \ 0 \ 0]^T, \mathbf{s}_{o_1} = [\frac{l_3}{2} \ 0 \ 0]^T, \mathbf{R}_4 = \begin{bmatrix} 1 & 0 & 0 \\ 0 & 1 & 0 \\ 0 & 0 & 1 \end{bmatrix};$$

(4) Constraint equation for sliding pairs:

$$\mathbf{C}_s = \mathbf{r}_1 + \mathbf{R}_1 \mathbf{s}_{s_1} - \mathbf{r}_4 - \mathbf{R}_4 \mathbf{s}_{s_4} = \mathbf{0}_{2 \times 1}, \tag{23}$$

the vectors in the above equation can be written as follows:

$$\mathbf{s}_{s_1} = \left[ \sqrt{l_3^2 - l_2^2 \sin^2 \gamma_2 - (z_4 - l_2 \cos \gamma_2)^2} \ 0 \ -0.12 \right]^T, \mathbf{R}_4 = \begin{bmatrix} 1 & 0 & 0 \\ 0 & 1 & 0 \\ 0 & 0 & 1 \end{bmatrix}, \mathbf{s}_{s_4} = [0 \ 0 \ 0]^T,$$

and the local degree of freedom as follows:

$$\mathbf{C}' = \gamma_3 = \mathbf{0}_{1 \times 1}. \tag{24}$$

Therefore, without considering the mechanism clearance, the constraint equation of the mechanism is:

$$\mathbf{C} = \begin{bmatrix} \mathbf{C}_o^T \\ \mathbf{C}_A^T \\ \mathbf{C}_B^T \\ \mathbf{C}_s^T \\ \mathbf{C}' \end{bmatrix} = \mathbf{0}_{12 \times 1}. \tag{25}$$

#### 4.2. Dynamic Model of Multi-Clearance Mechanism without Coating

Take the first time derivative and second time derivative of Equation (25), and obtain the velocity and acceleration constraint equations of the space four-bar mechanism:

$$\mathbf{C}_q \dot{\mathbf{q}} = \mathbf{v}, \tag{26}$$

$$\mathbf{C}_q \ddot{\mathbf{q}} = \boldsymbol{\gamma}, \tag{27}$$

where  $\mathbf{C}_q$  is the Jacobian matrix of the mechanism.  $\mathbf{v}$  and  $\boldsymbol{\gamma}$  are the functions that include velocity, displacement, and time. Substituting the above equation into Equation (5), use the Baumgarte method to consider the problem of constraint violation, set  $\alpha = \beta = 50$  [18], and the ideal joint dynamic equation of the four-bar mechanism can be obtained:

$$\begin{bmatrix} \mathbf{M} & \mathbf{C}_q^T \\ \mathbf{C}_q & \mathbf{0} \end{bmatrix}_{24 \times 24} \begin{bmatrix} \ddot{\mathbf{q}} \\ \boldsymbol{\lambda} \end{bmatrix}_{24 \times 1} = \begin{bmatrix} \mathbf{Q}_e \\ \boldsymbol{\gamma} - 2\alpha \dot{\mathbf{C}} - \beta^2 \mathbf{C} \end{bmatrix}_{24 \times 1}. \tag{28}$$

When the mechanism considers the existence of clearance at spherical joint-1, the ideal spherical joint constraint relationship between point A and point B is replaced by

the contact-impact forces  $\mathbf{F}_A$  and  $\mathbf{F}_B$ , and the dynamic equation of spherical joint-1 with clearance can be obtained:

$$\begin{bmatrix} \mathbf{M} & \mathbf{C}_q^T \\ \mathbf{C}_q & \mathbf{0} \end{bmatrix}_{18 \times 18} \begin{bmatrix} \ddot{\mathbf{q}} \\ \lambda \end{bmatrix}_{18 \times 1} = \begin{bmatrix} \mathbf{Q}_e + \mathbf{F}_A + \mathbf{F}_B \\ \gamma - 2\alpha\dot{\mathbf{C}} - \beta^2\mathbf{C} \end{bmatrix}_{18 \times 1}. \quad (29)$$

In order to investigate the effects of the number of spherical joint clearances and coatings on the dynamics and joint wear of a space deployable mechanism, a space four-bar mechanism consisting of one rotating pair, two spherical joints, and one sliding pair is also selected as the research object. The structural diagram, geometric parameters, and simulation parameters are shown in Figure 7 and Tables 2 and 3. The initial position of the crank centroid is (0, 0, and  $-1$ ), the crank speed is 60 r/min, and the positions of the spherical joint clearances are marked.

#### 1. Dynamics of multi-clearance mechanisms without coating

The RSSP mechanism consists of one rotating pair, two spherical joints, and one sliding pair. The positions of the clearances of the two spherical joints are marked in Figure 7. For convenience of description, they are named spherical joint-1 and spherical joint-2, respectively. The fourth-order Runge–Kutta method is used to simulate the dynamics of the clearances of two spherical joints with coating, with an initial step size of  $10^{-5}$  and a minimum step size of  $10^{-7}$ . The simulation parameters are listed in Table 3, and the specific calculation process is demonstrated in Figure 8.

- (i) The vector matrixes and joint constraint equations of various components in the global coordinate system are determined according to the model parameters and structural parameters of the mechanism considering joints with clearances, the coefficient matrixes in Equation (25) are determined, and they are sorted in MATLAB;
- (ii) For the solution of the dynamics of the mechanism, the velocity and acceleration of the mechanism at time  $t$  are determined according to the initial position and driving conditions of the mechanism. The obtained velocity and acceleration are taken as the position and velocity terms at time  $t + \Delta t$ . Then, the calculation result of  $\delta$  in Equation (4) is used to determine the contact states of the ball and shell in the spherical joint at a given time  $t + \Delta t$ ;
- (iii) When the contact collision depth is reached  $\delta \geq 0$ , the ball and shell are in contact or collision state. By combining the variable stiffness coefficient considering coating in Table 1 and the viscous damping term, the normal contact force  $F_n$  can be obtained, and the tangential contact force  $F_t$  can be obtained according to the improved Coulomb friction model. See [19] for a detailed calculation;
- (iv) By converting the contact-impact force acting on the contact impact point to the centroid of the component through Equations (6) and (7), the contact-impact force  $\mathbf{F}$  at the solution moment  $t + \Delta t$  can be obtained;
- (v) Substitute the contact-impact force into the dynamic Equation (29) considering the spherical joint clearances, obtain the acceleration at moment  $t + 2\Delta t$ , and determine the contact state between the ball and the shell at moment  $t + 2\Delta t$ ;
- (vi) Repeat the above steps (ii–v) until the end of the simulation.

In order to investigate the dynamic characteristics of the mechanism under the influence of multiple-clearance joints, the changes in the position, velocity, and acceleration of the slider when the space four-bar mechanism contains one spherical joint clearance and two spherical joint clearances are analyzed. Moreover, the obtained curves are compared with the dynamic results of the space four-bar mechanism in the ideal state. The results are shown in Figure 9.

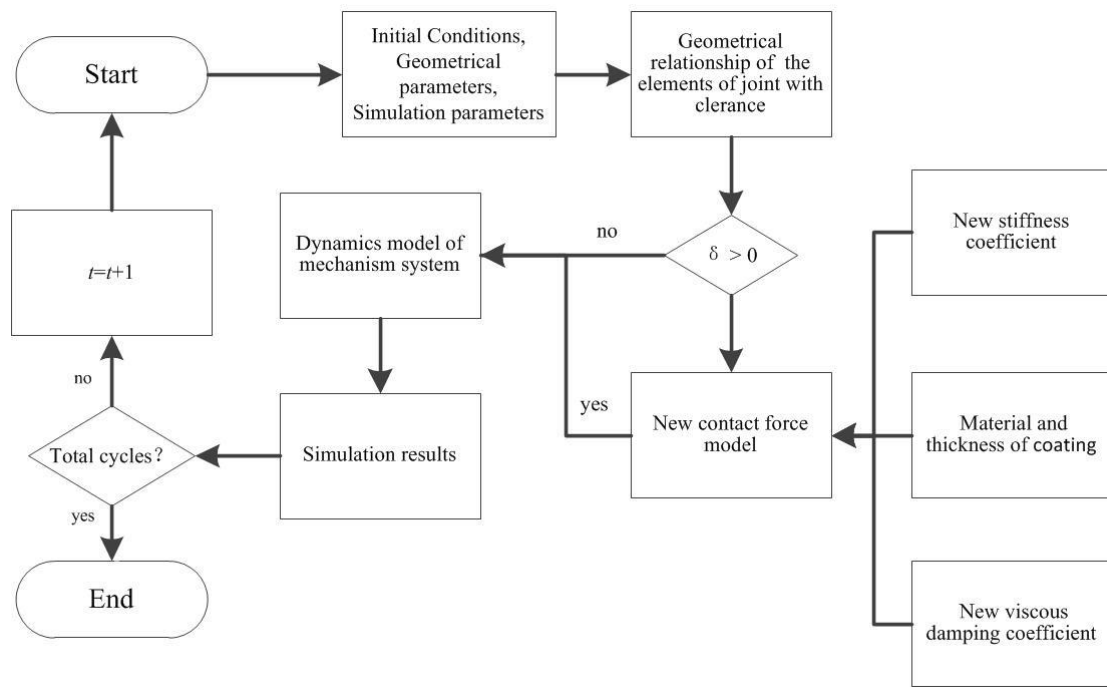


Figure 8. Flow chart of the dynamic calculation of the mechanism with clearance joints and coating.

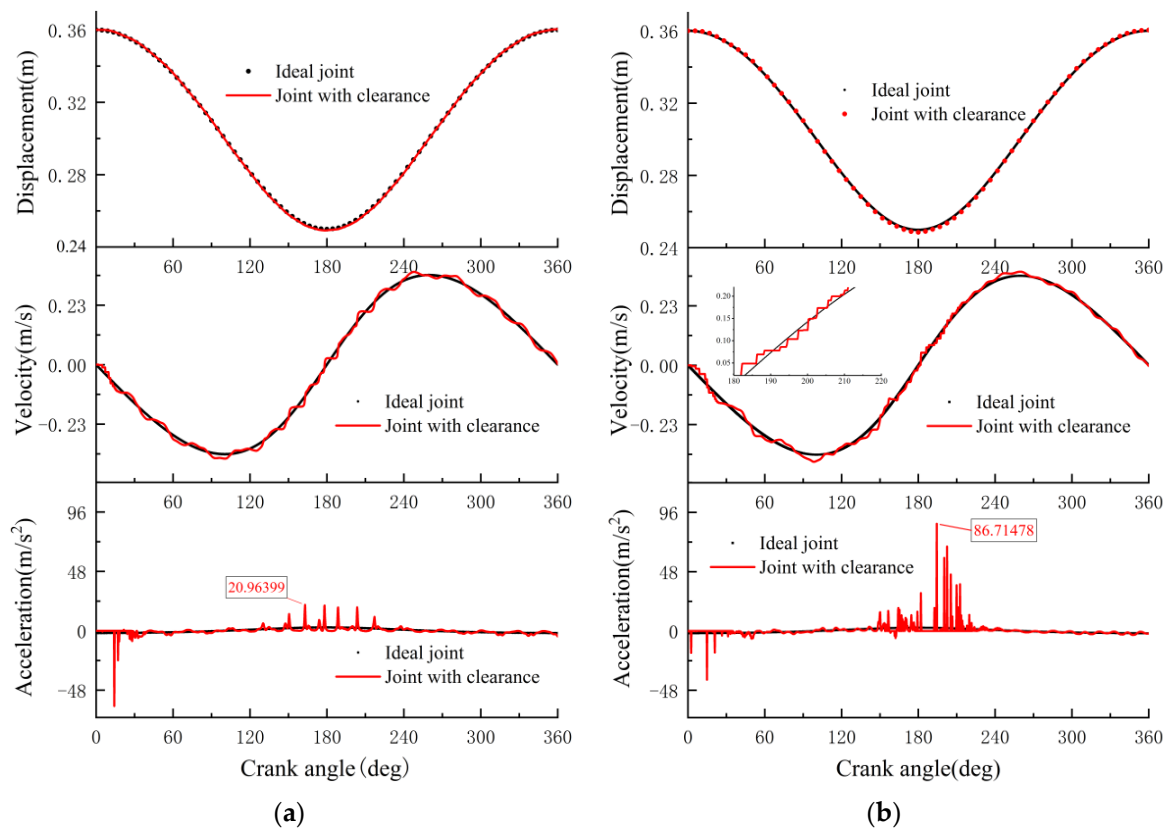


Figure 9. The dynamic characteristic curve of the space four-bar mechanism: (a) one clearance and (b) two clearances.

**Table 2.** The structure parameters of the mechanism.

Name	Length (m)	Mass (kg)	Moment of Inertia (kg·m <sup>2</sup> )		
			I <sub>xx</sub>	I <sub>yy</sub>	I <sub>zz</sub>
Crank	0.14	1.3	0.0001	0.0001	0.0001
Connecting rod	0.38	1.2	0.00001	0.00001	0.00001
Slider	-	2.2	-	-	-

**Table 3.** Simulation parameters for the mechanism.

Parameters	Name	Value	Parameters	Name	Value
Restitution coefficient $c_r$		0.7	Actuating speed	60 r/min	
Radius of socket		15 mm	Radius of ball	14.75 mm	
Linear wear coefficient [2]		$8 \times 10^{-14}$	Friction coefficient	Steel	0.01
Thickness	Coating	0.1 mm		MoS <sub>2</sub>	0.05
	Base	4.9 mm		Lead	0.08
Timespan		1 s		PTEE	0.167
Initial time step		$1 \times 10^{-5}$ s	Correction coefficients		$\alpha = \beta = 5$
Poisson's ratio	Steel	$\nu = 0.3$	Young's modulus	Steel	207 Gpa
	MoS <sub>2</sub>	$\nu = 0.29$		MoS <sub>2</sub>	110 Gpa
	Lead	$\nu = 0.42$		Lead	16.5 Gpa
	PTEE	$\nu = 0.4$		PTEE	2.86 Gpa

According to the results in Figure 9, the single spherical joint clearance and the two spherical joint clearances have almost no effect on the position change curve of the slider but have a more significant impact on the trend of speed change. As the number of clearances increases, the jumping frequency and amplitude of the slider speed increase, which is closely related to the increase in contact frequency when the mechanism considers multiple clearances. In comparison, the acceleration change curves of the slider present the greatest differences. Without considering the influence of the initial singular configuration, the maximum amplitude of the slider acceleration of the mechanism considering two spherical joint clearances is increased to four times that of the mechanism considering one spherical joint clearance. Obviously, this shows the same trend as the change in slider acceleration after the increase in clearances or the driving speed discussed in Section 5, and more frequent contact collisions will also exacerbate the vibration of the mechanism.

Combining the calculation methods for the joint reaction force or contact-impact force of the spherical joint clearance in Sections 2 and 4 of this paper, the joint reaction forces in the following three situations are compared: ideal spherical joint, spherical joint clearance-1 + ideal spherical joint-2, and spherical joint clearance-1 + spherical joint clearance-2. The contact-impact force  $F_c$  and its components  $F_{cx}$ ,  $F_{cy}$ , and  $F_{cz}$  are as shown in Figure 10, and the two spherical joints have the same parameters and clearance size. It can be seen that as the number of clearances increases, the amplitude of the joint reaction force at the spherical joint-1 increases significantly, the acceleration change in the initial stage of motion becomes more obvious, and the frequency change trend is basically consistent. According to the above information, it can be seen that under the same working conditions, the number of joint clearances has a significant impact on the dynamic results of the actuator of the mechanism, but it is not a linear superposition of the effects of the spherical joint clearances. The calculation of the reaction force at the spherical joint-1 can provide data support for the calculation of the wear amount of the spherical joint in the global coordinate system in different directions.

## 2. Calculation of joint wear of the multi-clearance mechanism without coating

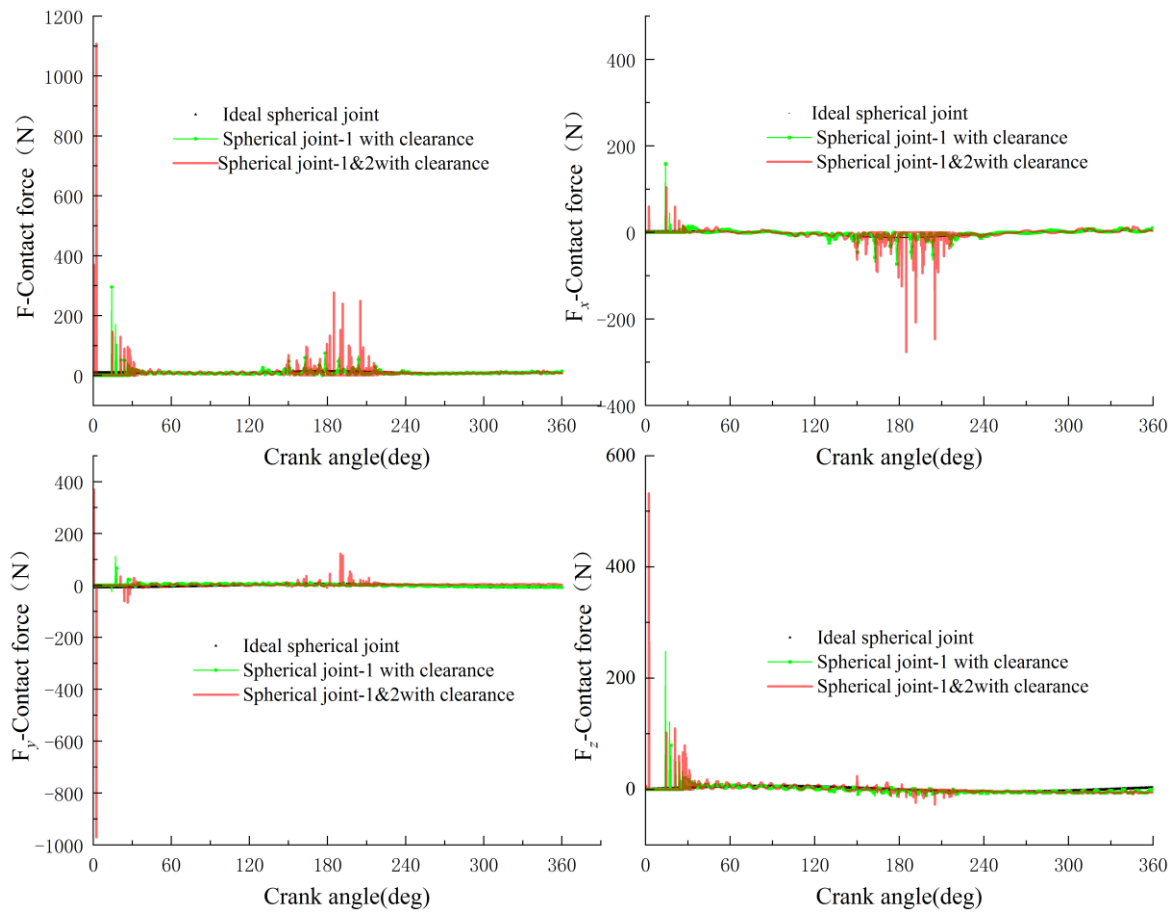


Figure 10. Reaction force of sphere joints 1.

Based on the dynamics of multi-clearance mechanisms, the Archard model is employed to calculate the wear amount of the mechanism, considering a single spherical joint clearance and two spherical joint clearances. The calculation results are shown in Figure 11, in which the 3D gradient map represents the wear amounts in various vector directions under the three normal components of the contact force within 0–1 s, and the coordinate axes represent the angular displacement, time, and wear amount, respectively. The distribution of wear amount within the rotation angle in various directions during the entire rotation cycle of the mechanism is displayed by a polar coordinate diagram, and the change curve shown in red represents the inner surface profile of the worn spherical shell.

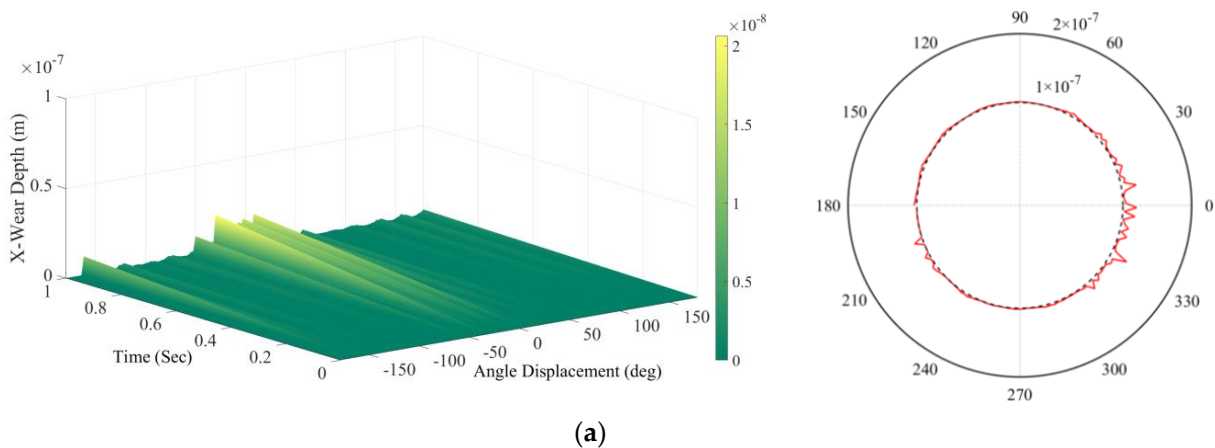
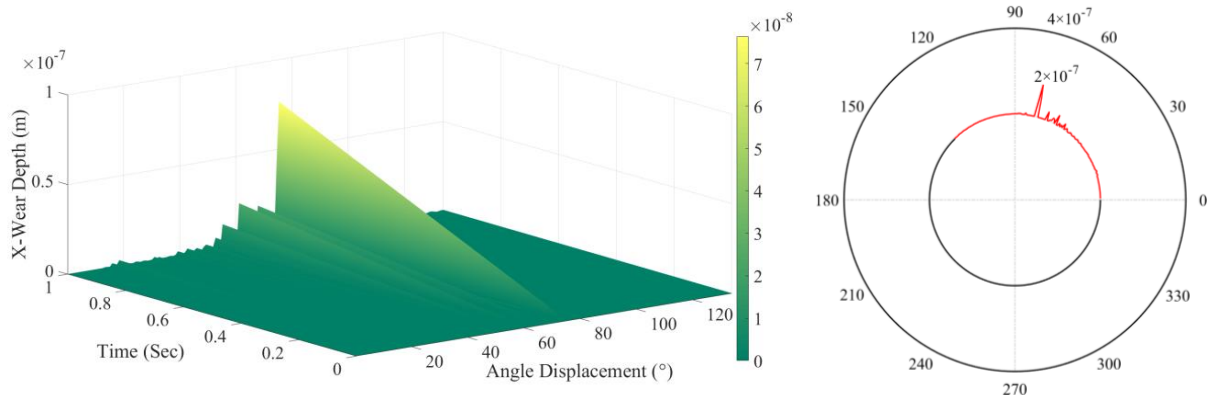
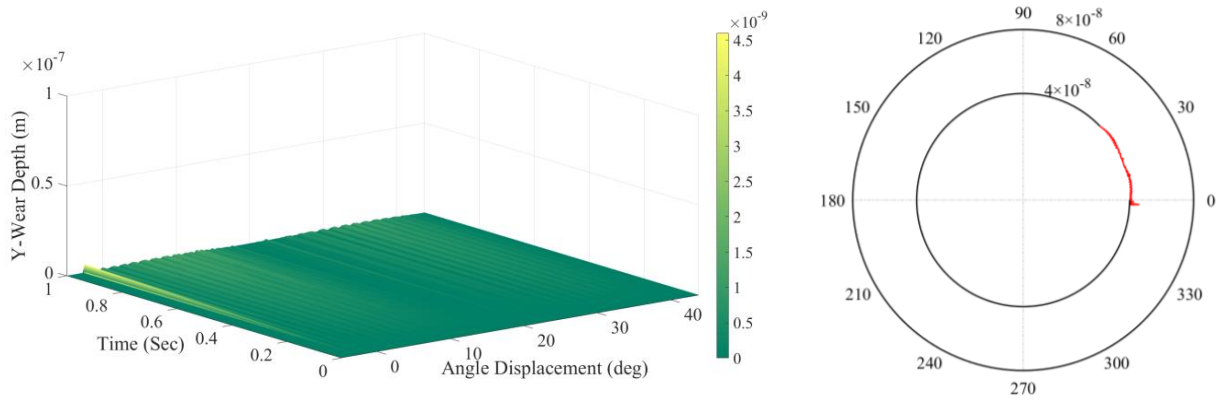


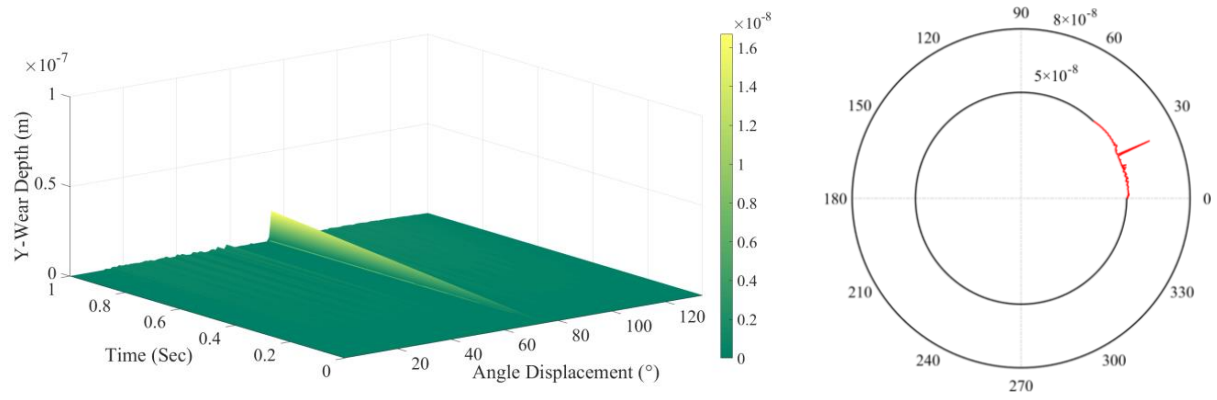
Figure 11. Cont.



(b)



(c)



(d)

Figure 11. Cont.

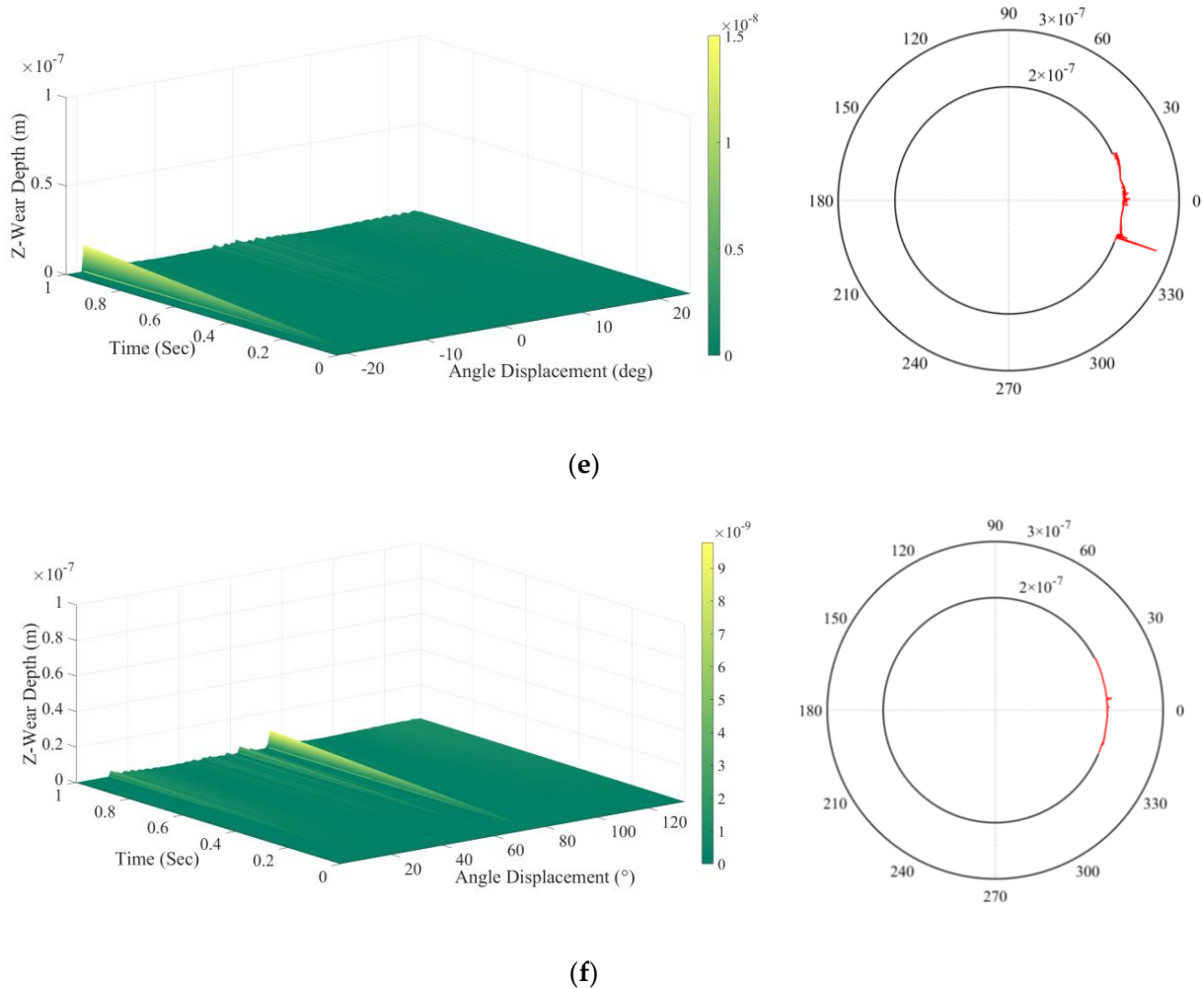


**Figure 11.** Influence of clearance number on wear performance: (a) one clearance  $x$ -direction; (b) two clearances  $x$ -direction; (c) one clearance  $y$ -direction; (d) two clearances  $y$ -direction; (e) one clearance  $z$ -direction; and (f) two clearances  $z$ -direction.

The space four-bar mechanism containing one spherical joint clearance is compared with that containing two spherical joint clearances, and the wear depth, maximum wear angle, minimum wear angle, and wear range in different directions at the spherical joint-1 are compared. The specific results are listed in Table 4. When the mechanism involves multiple clearances, with the increase of the clearance number, the clearance collision becomes more severe, and the wear at the joint with clearance also intensifies. Figure 11a,c,e show the change in wear amount in the  $x$ ,  $y$ , and  $z$  directions when there is clearance at the spherical joint clearance-1. The ball rotates around  $x$  nearly in the whole cycle, so the clearance wear area is close to  $2\pi$ , and the wear in the  $-150^\circ \sim 50^\circ$  area is the most severe, which is mainly because when the crank is turned around  $180^\circ$ , the mechanism is close to the singular configuration. The wear in the  $y$  and  $z$  directions does not change significantly except in the initial stage. Figure 11b,d,f show the change in wear amount in the  $x$ ,  $y$ , and  $z$  directions when the spherical joint clearance-1 and the spherical joint clearance-2 exist at the same time. Obviously, compared with the single clearance situation, the wear amount in the half-cycle region has increased significantly in the  $x$  and  $y$  directions. With the increase in the number of spherical joint clearances, the variable topology probability of the mechanism motion increases, the motion uncertainty increases, the wear area changes from full-cycle wear to local wear, and the maximum wear amount increases. The rotation angle regions of wear in the  $y$  and  $z$  directions are basically unchanged. At the same time, according to the results in Table 4, compared with the case containing only one spherical

joint clearance, the wear amount in the z direction at spherical joint-1 does not increase with the increase in clearances but decreases slightly, indicating that the contact frequency in the z direction decreases with the increase in the number of spherical joint clearances, which mainly depends on the structural characteristics of the mechanism. This result is consistent with the change rule of wear amount concluded in different directions in [21,23,29].

**Table 4.** Wear prediction without coating.

Number of Clearance	Wear Direction	Max Wear Depth (m)	Max Wear Angle (deg)	Min Wear Angle (deg)	Wear Range (deg)
1	x	$7.5000 \times 10^{-9}$	179.9386	-179.9454	359.8840
1	y	$7.2306 \times 10^{-12}$	44.0792	-4.9569	49.0361
1	z	$5.1508 \times 10^{-11}$	24.1878	-21.4257	45.6135
2	x	$8.3004 \times 10^{-11}$	134.6607	0	134.6607
2	y	$2.7420 \times 10^{-11}$	46.7107	-5.427	52.1377
2	z	$1.2251 \times 10^{-10}$	27.7638	-22.6586	50.4224

#### 4.3. Multi-Clearance Mechanism with Coating

##### 1. Dynamic simulation of the multi-clearance mechanism with coating

In order to investigate the effect of coating on the vibration characteristics of the multi-clearance mechanism, the dynamic results of the slider are calculated in the following three situations: a single spherical joint clearance without coating, two spherical joint clearances with one coating, and two spherical joint clearances with two coatings. Poly-tetrafluoroethylene (PTFE) is used as the coating material, and the coating thickness and substrate thickness are shown in Table 3. The contact force model considering the variable stiffness coefficient of the coating material and the spherical joint in Table 1 is selected to carry out dynamic simulation, and the results are shown in Figure 12.

Figure 12b shows an enlarged image of the left part. According to the simulation results, with the increase in clearances in the mechanism, the contact collision frequency of the mechanism is intensified, and the contact force or acceleration amplitude between contact elements increases, which is consistent with the conclusion drawn in previous works. At the same time, the addition of coating can significantly reduce the acceleration amplitude, and in the mechanism with two clearances, the effect of coating is particularly significant. The main reason is that the acceleration amplitude of the slider is relatively large in the case of two clearances, and when the coating is added to the slider clearance, the dynamic performance of the slider benefits the most. To analyze the effects of coating quantity on the dynamics of the mechanism, the dynamic results of the slider when the mechanism contains spherical joint clearances but with different numbers of coatings are compared. Specifically, both spherical joint 1 and spherical joint 2 have clearances; the results of applying coating to spherical joint 1, applying coating to spherical joint 2, and applying coating to both spherical joints are discussed; and some rotation angle areas of the crank are enlarged, as shown in Figure 13. The results are compared with situations when both spherical joint clearances have coatings. When the space four-bar mechanism contains two spherical joints 1 and 2 with clearances, different applications of coatings have a significant different impact on the mechanism. When the clearance of spherical joint 1 has a coating, the acceleration trend of the slider is basically the same as when the clearances of both spherical joints have coatings, and the amplitude of the change is not significantly different. However, when the clearance of spherical joint 2 has coating, but the clearance of spherical joint 1 has no coating, the acceleration change of the slider increases more significantly compared to when coating is considered for both spherical joints. The difference is most significant at the initial stage and when the crank has turned to near 180°, as shown in Figure 13b, which is mainly due to the structural characteristics of the mechanism in series connection. Therefore, in a multi-clearance mechanism, when the same material and parameters are chosen for each clearance, the coating in the clearance

of the non-actuator has no significant influence on the dynamic results of the actuator. As a result, in order to reduce processing costs and process flow and address the vibration caused by clearance in the series space deployable mechanism, priority should be given to adding solid lubricating coatings at the joints of the actuator.

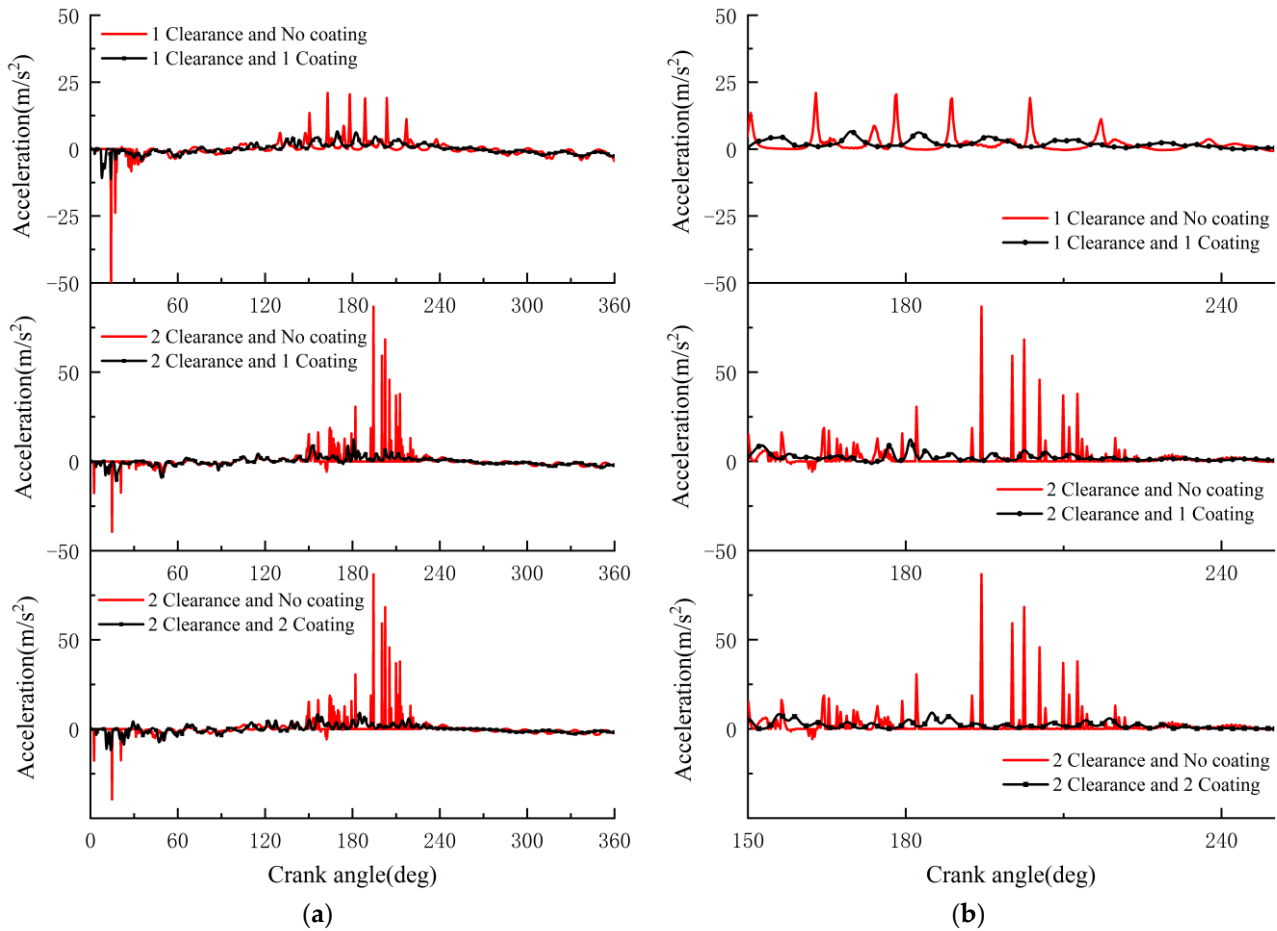


Figure 12. Influence of coating and clearance on dynamics.

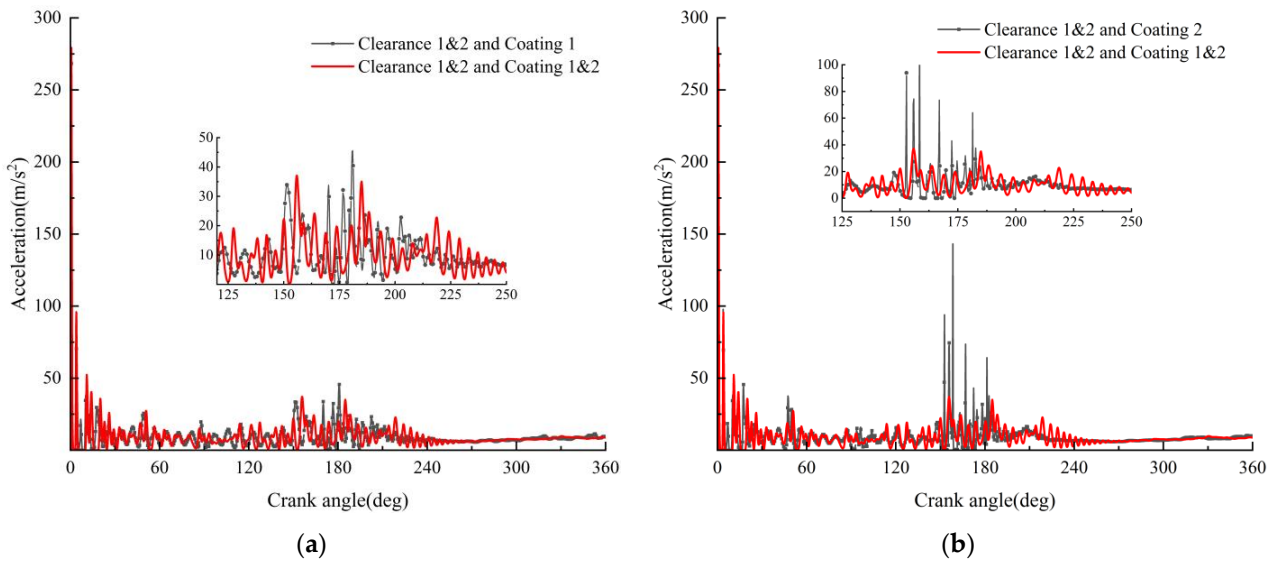


Figure 13. Influence of coating on dynamics: (a) clearance 1 and 2 and coating 1 (b) clearance 1 and 2 and coating 2.

The reaction forces  $F$ ,  $F_x$ ,  $F_y$ , and  $F_z$  at the rotating pair joint and the contact-impact forces  $F_c$ ,  $F_{cx}$ ,  $F_{cy}$ , and  $F_{cz}$  at the spherical joint-1 of the following three situations are compared: ideal spherical joint, spherical joint with clearance-1 + ideal spherical joint-2, and spherical joint with clearance-1 + spherical joint with clearance-2, as shown in Figures 14 and 15. According to the simulation results, with the increase in clearance number, the reaction forces at the rotating pair joint and the contact-impact forces at spherical joint-1 grow significantly. The calculation of the contact-impact force and its components after applying coatings to different spherical joint clearances can provide data support for the calculation of joint wear considering clearance with coating.

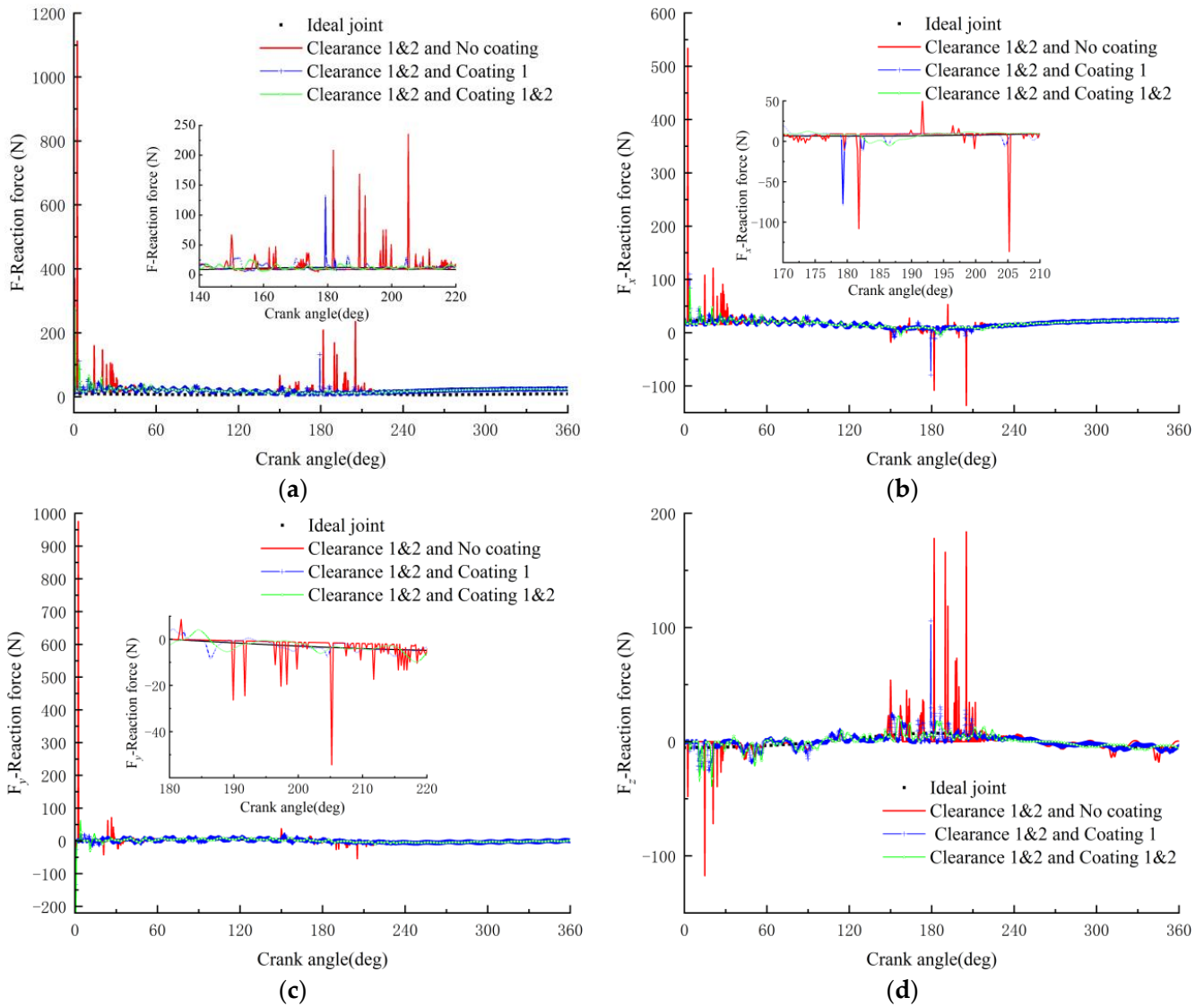
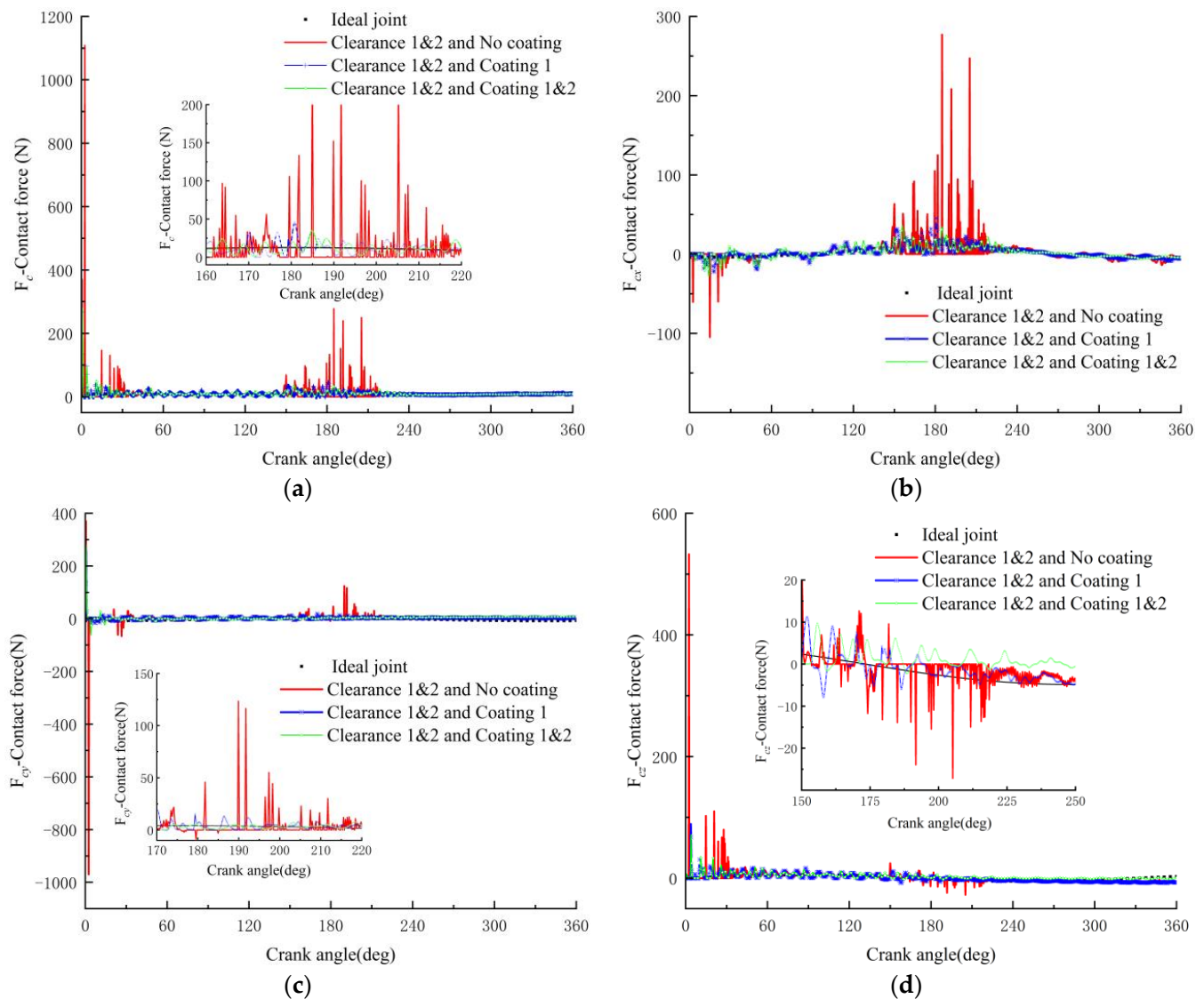


Figure 14. Reaction force of revolute joints considering coating.



**Figure 15.** Contact force of sphere joints-1 considering coating.

## 2. Calculation of joint wear of the multi-clearance mechanism with coating

By considering the impact of both coating and multiple clearances on the dynamics of the mechanism, dynamic simulations are conducted in three cases: two clearances without coating, two clearances with one coating, and two clearances with two coatings. According to the distribution of wear amount at the rotation angles of the shell in various directions during the full-cycle rotation, the wear depth changes of the spherical joint associated with the slider under three working conditions are compared and analyzed using the 3D diagram and polar coordinates of wear amount in different directions. The simulation results are shown in Figure 16.

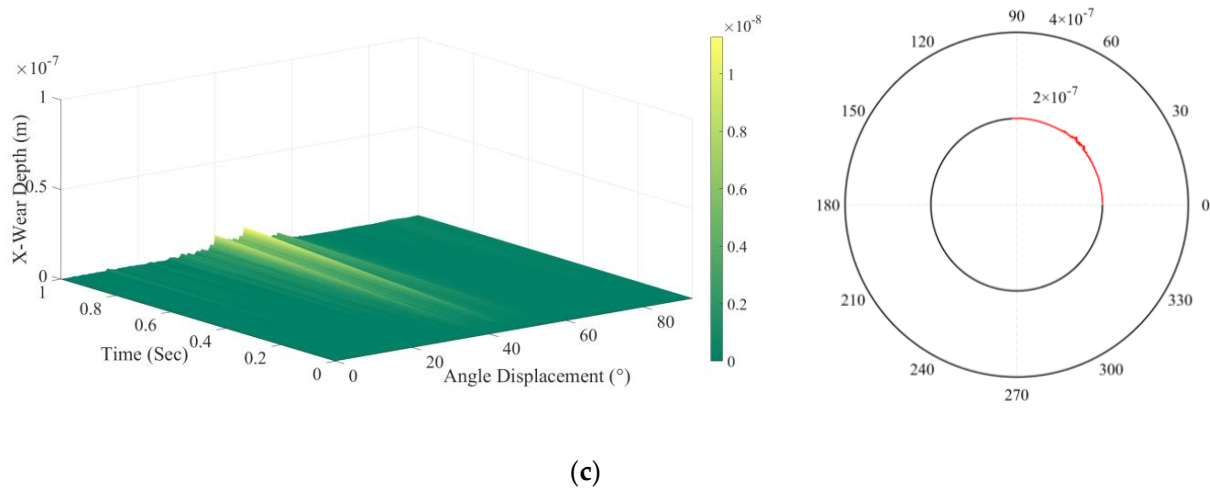
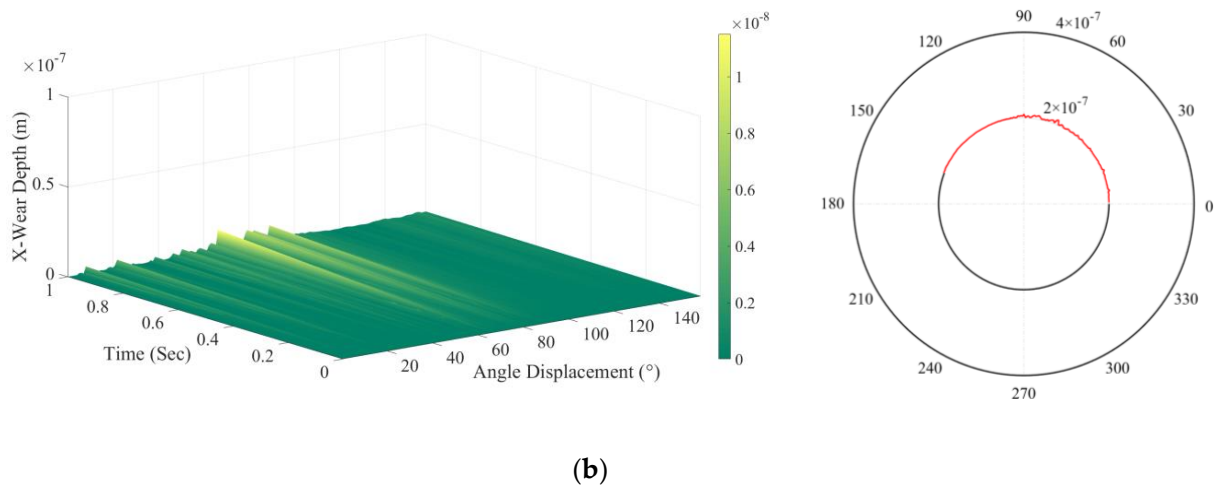
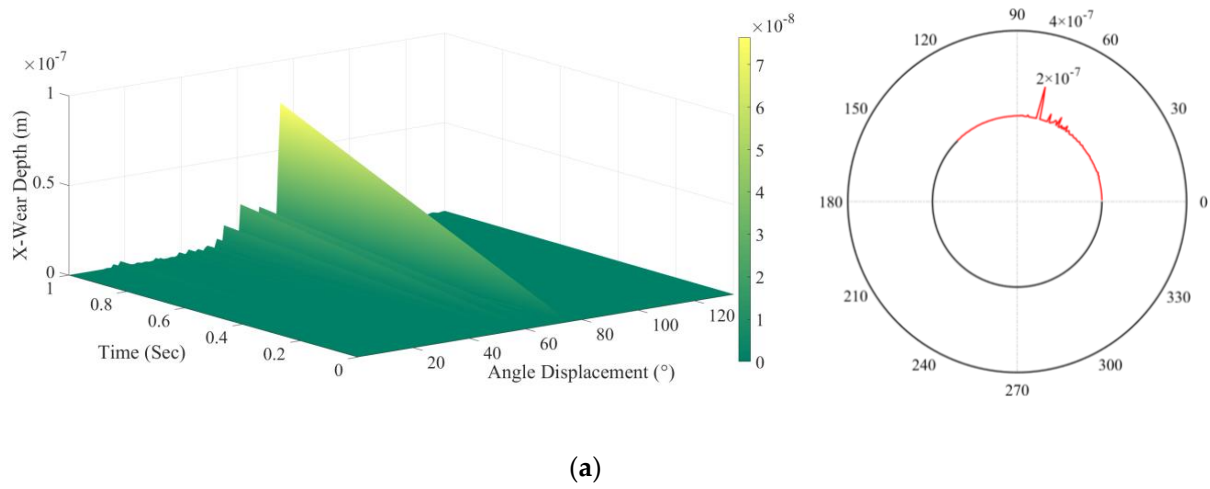


Figure 16. Cont.

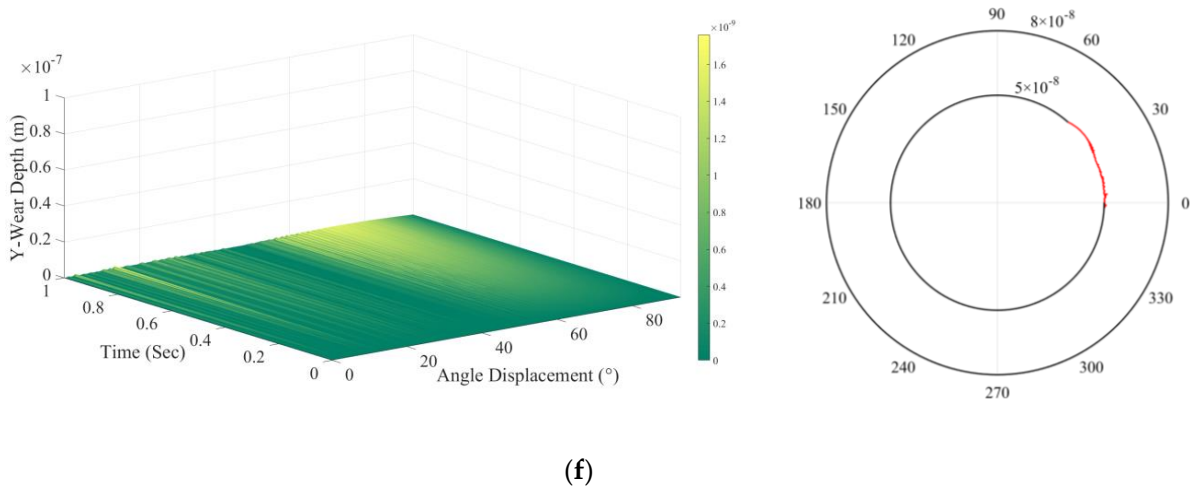
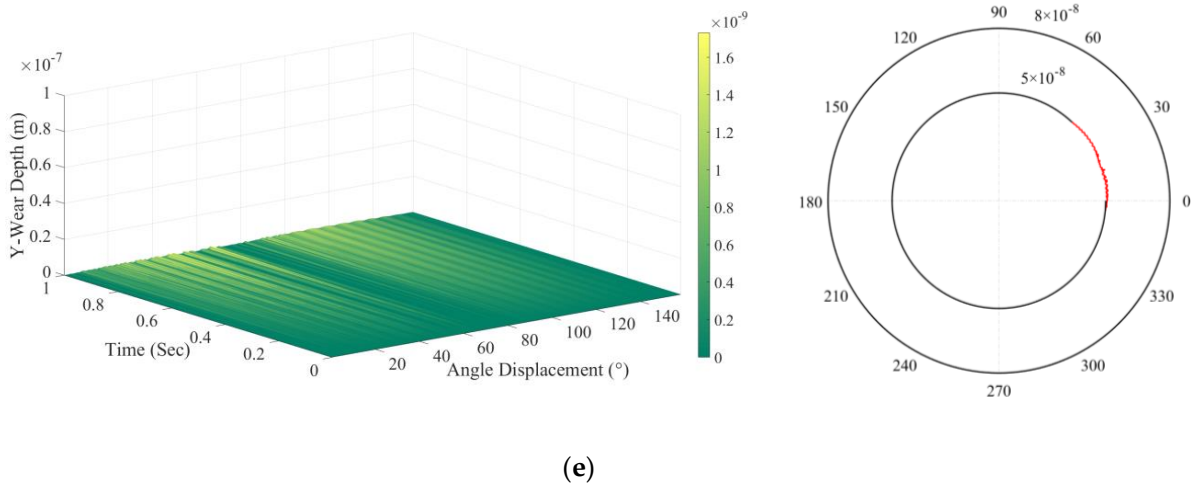
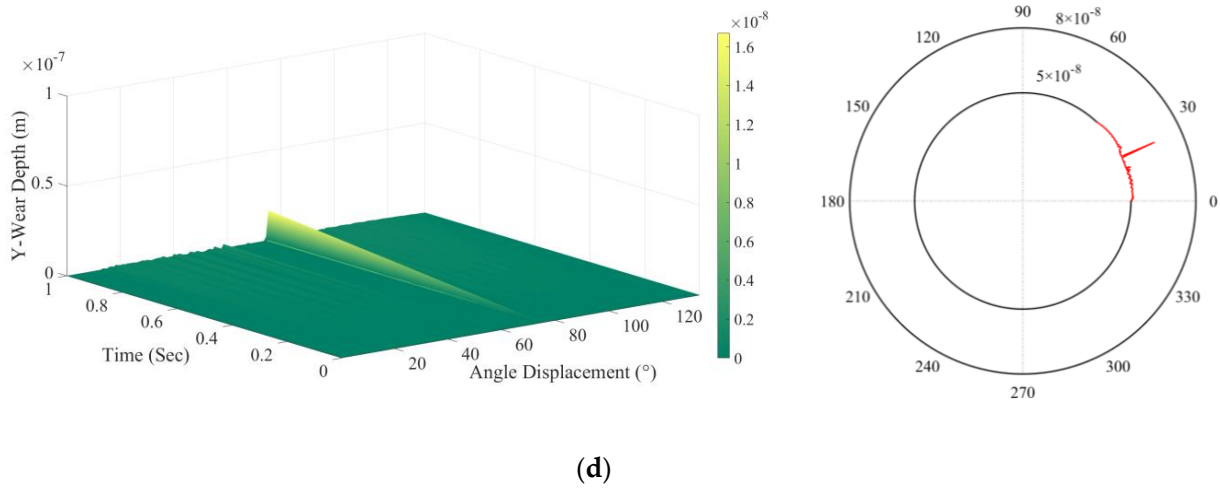
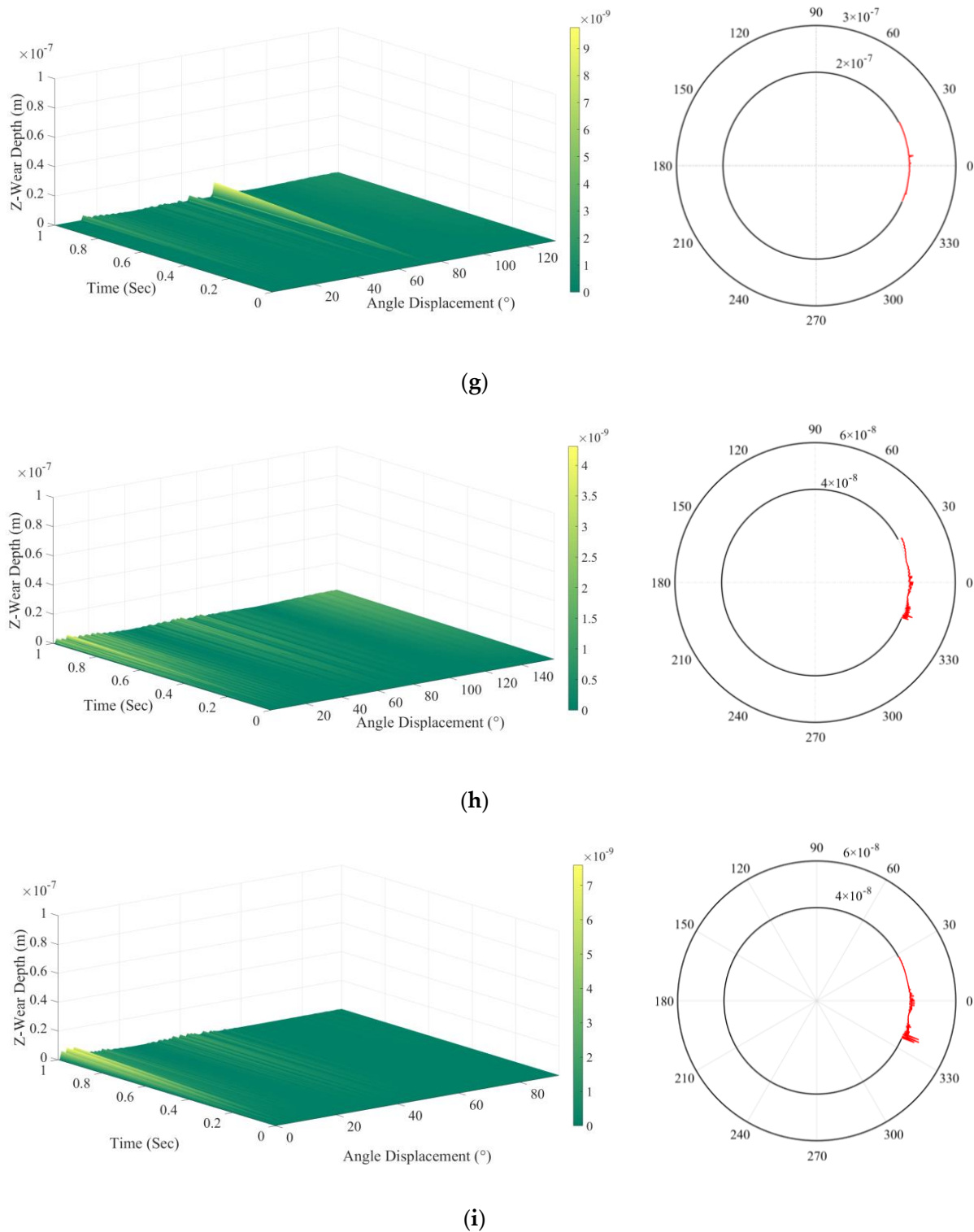


Figure 16. Cont.



**Figure 16.** Influence of clearance number on wear performance: (a) 2 clearances and no coating in  $x$ -direction; (b) 2 clearances and 1 coating in  $x$ -direction; (c) 2 clearances and 2 coating in  $x$ -direction; (d) 2 clearances and no coating in  $y$ -direction; (e) 2 clearances and 1 coating in  $y$ -direction; (f) 2 clearances and 2 coating in  $y$ -direction; (g) 2 clearances and 2 coating in  $z$ -direction; (h) 2 clearances and 1 coating in  $z$ -direction; (i) 2 clearances and 2 coating in  $z$ -direction.

The effects of the number of clearances on the dynamic performance and wear amount of the mechanism have been discussed above, so the case of one clearance is not compared

with that of two clearances. At the same time, when considering coatings for two clearances, in order to better carry out the damping effect of the coating, the coating should be applied to the clearance of the actuator. If there is no clearance in the actuator, it should be applied to the clearance joint near the actuator. Table 5 shows the wear depth, maximum wear angle, minimum wear angle, and wear range of the mechanism containing two spherical joint clearances and different numbers of coatings. Table 6 shows the changes in wear depth and wear range of a spaced four-bar mechanism containing two spherical joint clearances with different coating quantities and without coating. Combining Figure 16, the numerical dynamics results of the mechanism with multi-clearance joints under the influence of different coatings are compared and analyzed, and the results are as follows: (i) from Figure 16a,d,g to Figure 16b,e,h, it can be seen that application of coating to the clearance joint can significantly improve the wear condition at the clearance joints; the wear amount in each rotation direction of the spherical joint decreases, with the most significant decrease in the  $x$  direction, which is because the contact-impact force of the slider in the  $x$  direction is the largest, so it is most affected by the coating; (ii) according to Figure 16c,f,i and the previous discussion, the effect of coating quantity on the dynamics of the mechanism is related to the characteristics of the mechanism. When the space four-bar mechanism has coatings at the clearances of two spherical joints and only has coating at spherical joint-1, the contact-impact force at the spherical joint-1 does not change much, so the wear depth slightly decreases in the  $x$  direction for about  $7.7 \times 10^{-12}$ , while the wear amount in the  $y$  and  $z$  directions remains basically unchanged; and (iii) when the number of clearances and the coating material and thickness remain unchanged, the wear ranges in the  $x$  direction are compared in the three cases of one coating, two coatings, and no coating. Compared with the situation of no coating, in which the wear range increases by  $24.38^\circ$ , after applying coating, the wear range decreases by  $41.17^\circ$ , for a difference of  $65.55^\circ$ . The wear range is significantly reduced, while the wear range in the  $y$  and  $z$  directions remains basically unchanged.

**Table 5.** Wear prediction with coating.

Number of Coating	Wear Direction	Max Wear Depth (m)	Max Wear Angle (deg)	Min Wear Angle (deg)	Wear Range (deg)
1	$x$	$2.0485 \times 10^{-11}$	159.0376	0	159.0376
1	$y$	$1.9297 \times 10^{-12}$	46.7685	-6.1449	52.9134
1	$z$	$1.9763 \times 10^{-11}$	27.5031	-22.7086	50.2117
2	$x$	$1.2828 \times 10^{-11}$	93.3712	-0.1231	93.4943
2	$y$	$2.6656 \times 10^{-12}$	48.5997	-3.3626	51.9623
2	$z$	$1.6656 \times 10^{-11}$	28.0459	-24.0083	52.0542

**Table 6.** Comparison of wear prediction.

Number of Coating	Wear Direction	Reduction of Max Wear Depth (m)	Percentage of Reduction	Reduction of Wear Range (deg)	Percentage of Increment
1	$x$	$6.25 \times 10^{-11}$	75.32%	-24.38	-18.10%
1	$y$	$2.55 \times 10^{-11}$	92.96%	-0.78	-1.49%
1	$z$	$1.03 \times 10^{-10}$	83.87%	0.21	0.42%
2	$x$	$7.02 \times 10^{-11}$	84.55%	41.17	30.57%
2	$y$	$2.48 \times 10^{-11}$	90.28%	0.18	0.34%
2	$z$	$1.06 \times 10^{-10}$	86.40%	-1.63	-3.24%

## 5. Conclusions

On the basis of previous research on the dynamics of mechanisms considering coating and single spherical joint clearance, this paper considers the influence of multiple clearances on mechanism dynamics, the effectiveness of coating in reducing the vibration of the multi-clearance mechanism, and the effects of solid lubricant in reducing the wear of

mechanism joints. With the space bar mechanism containing coating and two spherical joint clearances as examples, the study is carried out on the three aspects of the kinematics of mechanisms containing clearances, the dynamics of mechanisms containing clearances, and the calculation of joint clearance wear, and the results show that:

- (1) After applying coatings to different spherical joint clearances, the acceleration amplitude of the slider decreases at different clearance sizes, and the reduction extent in the acceleration amplitude of the actuator varies. However, the vibration of the mechanism is alleviated, verifying the effectiveness of coating application in reducing the vibration of the mechanism considering spherical joint clearances;
- (2) By comparing the 3D gradient maps and polar coordinates of the wear depth, as well as the changes in maximum wear amount and wear area in each vector direction, it can be seen that after applying coating, the wear amount of the spherical joint clearance in each vector direction is significantly reduced, and the rotation angle wear area is slightly increased compared to when no coating is applied. This conclusion is consistent with the results in [18];
- (3) When the properties and geometric parameters of the coating materials used in the joints of the system with a multi-clearance mechanism are unchanged, the effect of coating on the dynamic results of the non-executing member is not obvious. In order to reduce the cost and shorten the working cycle, it can be given priority to add a solid lubrication coating at the joint of the actuator, which can provide ideas for the process design, lubrication, and vibration reduction strategy of the mechanism system;
- (4) The consideration of the effect of coating on the dynamics and wear calculation of multi-clearance mechanisms provides ideas for the vibration reduction and wear reduction of mechanisms under actual working conditions. Meanwhile, this research on the dynamics of multi-clearance mechanisms has laid a solid theoretical foundation for subsequent experiments on the dynamics of clearance mechanisms considering coatings.

**Author Contributions:** Methodology, Q.J.; Validation, H.L.; Data curation, Q.J.; Writing—original draft, Q.J.; Writing—review & editing, H.L. All authors have read and agreed to the published version of the manuscript.

**Funding:** This research was funded by [Gansu Natural Science Foundation] grant number [23JRRM737], [Gansu Agricultural Shortboard Foundation] grant number [njyf2023-06], and [Gansu University Innovation Foundation] grant number [2021B-277].

**Data Availability Statement:** Since much of the content in this paper is part of the team's ongoing research about joints and coatings, the relevant data cannot be shared for the moment.

**Conflicts of Interest:** The authors declare no conflict of interest.

## References

1. Yan, S.Z.; Xiang, W.W.K.; Huang, T.Q. Advances in Modeling of Clearance Joints and Dynamics of Mechanical Systems with Clearances. *Acta Sci. Nat. Univ. Pekin.* **2016**, *4*, 741–756.
2. Flores, P. Modeling and simulation of wear in revolute clearance joints in multibody systems. *Mech. Mach. Theory* **2009**, *44*, 1211–1222. [[CrossRef](#)]
3. Flores, P.; Lankarani, H.M. Spatial rigid-multibody systems with lubricated spherical clearance joints: Modeling and simulation. *Nonlinear Dyn.* **2009**, *60*, 99–114. [[CrossRef](#)]
4. Flores, P. A parametric study on the dynamic response of planar multibody systems with multiple clearance joints. *Nonlinear Dyn.* **2010**, *61*, 633–653. [[CrossRef](#)]
5. Muvengei, O.; Kihui, J.; Ikua, B. Numerical study of parametric effects on the dynamic response of planar multi-body systems with differently located frictionless revolute clearance joints. *Mech. Mach. Theory* **2012**, *53*, 30–49. [[CrossRef](#)]
6. Muvengei, O.; Kihui, J.; Ikua, B. Dynamic analysis of planar rigid-body mechanical systems with two-clearance revolute joints. *Nonlinear Dyn.* **2013**, *73*, 259–273. [[CrossRef](#)]
7. Varedi, S.M.; Daniali, H.M.; Dardel, M.; Fathi, A. Dynamic behavior analysis of a planar four bar linkage with three clearance joints. In Proceedings of the International Conference on Robotics and Mechatronics, Tehran, Iran, 15–17 October 2014; pp. 595–600.
8. Wang, X.; Lin, W.; Ji, X.; Gao, Z.; Bai, X.; Guo, Y. Dynamic analysis of a planar multibody system with multiple revolute clearance joints. *Proc. Inst. Mech. Eng. Part C J. Mech. Eng. Sci.* **2018**, *233*, 3429–3443. [[CrossRef](#)]

9. Geng, X.; Li, M.; Liu, Y.; Zheng, W.; Zhao, Z. Non-probabilistic kinematic reliability analysis of planar mechanisms with non-uniform revolute clearance joints. *Mech. Mach. Theory* **2019**, *140*, 413–433. [[CrossRef](#)]
10. Tan, H.; Hu, Y.; Li, L. A continuous analysis method of planar rigid-body mechanical systems with two revolute clearance joints. *Multibody Syst. Dyn.* **2016**, *40*, 347–373. [[CrossRef](#)]
11. Wang, T.C.; Chen, G.P.; Ma, F.; Sun, D.Y. Dynamic analysis of multibody systems with mixed clearance. *J. Vib. Shock* **2016**, *35*, 178–184.
12. Yu, H.; Zhang, J.; Wang, H. Dynamic performance of over-constrained planar mechanisms with multiple revolute clearance joints. *Proc. Inst. Mech. Eng. Part C J. Mech. Eng. Sci.* **2017**, *232*, 3524–3537. [[CrossRef](#)]
13. Song, N.; Peng, H.; Xu, X.; Wang, G. Modeling and simulation of a planar rigid multibody system with multiple revolute clearance joints based on variational inequality. *Mech. Mach. Theory* **2020**, *154*, 104053. [[CrossRef](#)]
14. Kou, B.; Li, Z.; Zhang, Z.; Li, R. Tribological Properties of ZrO<sub>2</sub> Coating on the Ball Joint of an Axial Piston Pump in High Water Based Emulsion Medium. *Math. Probl. Eng.* **2021**, *2021*, 9978006. [[CrossRef](#)]
15. Ambrósio, J.; Verissimo, P. Improved bushing models for general multibody systems and vehicle dynamics. *Multibody Syst. Dyn.* **2009**, *22*, 341–365. [[CrossRef](#)]
16. Rodrigues da Silva, M.; Marques, F.; Tavares da Silva, M.; Flores, P. A comparison of spherical joint models in the dynamic analysis of rigidmechanical systems ideal, dry, hydrodynamic and bushing approaches. *Multibody Syst. Dyn.* **2022**, *56*, 221–266. [[CrossRef](#)]
17. Almomani, M.A.; Fares, M.M.; Almesidien, E.M. Toward long live ceramic on ceramic hip joints in vitro investigation of squeaking of coated hip joint with layer by layer reinforced PVA coatings. *De Gruyter* **2022**, *22*, 522–535.
18. Li, Y.; Yang, Y.; Li, M.; Liu, Y.; Huang, Y. Dynamics analysis and wear prediction of rigid-flexible coupling deployable solar array system with clearance joints considering solid lubrication. *Mech. Syst. Signal Process.* **2022**, *162*, 108059. [[CrossRef](#)]
19. Jing, Q.; Liu, H. Dynamic analysis and wear calculation of space deployable mechanism considering spherical joints with clearance and coating. *Proc. Inst. Mech. Eng. Part C J. Mech. Eng. Sci.* **2023**, *237*, 2729–2752. [[CrossRef](#)]
20. Zhuang, X.; Yu, T.; Liu, J.; Song, B. Kinematic reliability evaluation of high-precision planar mechanisms experiencing non-uniform wear in revolute joints. *Mech. Syst. Signal Process.* **2022**, *169*, 108748. [[CrossRef](#)]
21. Wang, G.; Liu, H.; Deng, P. Dynamics Analysis of Spatial Multibody System with Spherical Joint Wear. *J. Tribol.* **2015**, *137*, 021605. [[CrossRef](#)]
22. Zhuang, X.; Afshari, S.S.; Yu, T.; Liang, X. A hybrid model for wear prediction of a single revolute joint considering a time-varying lubrication condition. *Wear* **2020**, *442–443*, 203124. [[CrossRef](#)]
23. Hou, Y.-L.; Deng, Y.-J.; Zeng, D.-X. Dynamic modelling and properties analysis of 3RSR parallel mechanism considering spherical joint clearance and wear. *J. Central South Univ.* **2021**, *28*, 712–727. [[CrossRef](#)]
24. Jing, Q.; Liu, H.Z. Dynamic characteristics of linkage mechanism considering clearance of cylinder pair. *J. Vib. Shock* **2021**, *40*, 32–39.
25. Jing, Q.; Liu, H.Z.; Wang, G.X. Analysis of the constraint reaction force in a mechanism system. *J. Vib. Shock* **2019**, *38*, 161–166.
26. Flores, P.; Machado, M.; Seabra, E.; Tavares da Silva, M. A Parametric Study on the Baumgarte Stabilization Method for Forward Dynamics of Constrained Multibody Systems. *J. Comput. Nonlinear Dyn.* **2011**, *6*, 011019. [[CrossRef](#)]
27. Archard, J.F. Contact and Rubbing of Flat Surfaces. *J. Appl. Phys.* **1953**, *24*, 981–988. [[CrossRef](#)]
28. Zhu, A.; He, S.; Zhao, J.; Luo, W. A nonlinear contact pressure distribution model for wear calculation of planar revolute joint with clearance. *Nonlinear Dyn.* **2016**, *88*, 315–328. [[CrossRef](#)]
29. Askari, E.; Flores, P.; Dabirrahmani, D.; Appleyard, R. Dynamic modeling and analysis of wear in spatial hard-on-hard couple hip replacements using multibody systems methodologies. *Nonlinear Dyn.* **2015**, *82*, 1039–1058. [[CrossRef](#)]

**Disclaimer/Publisher’s Note:** The statements, opinions and data contained in all publications are solely those of the individual author(s) and contributor(s) and not of MDPI and/or the editor(s). MDPI and/or the editor(s) disclaim responsibility for any injury to people or property resulting from any ideas, methods, instructions or products referred to in the content.